LBL-23177
Preprint

Lawrence Berkeley Laboratory
UNIVERSITY OF CALIFORNIA

Materials & Chemical Sciences Division

RECEIVED
LAWRENCE
BERKELEY LABORATORY

MAY 12 1987

LIBRARY AND
DOCUMENTS SECTION

Submitted to Journal of the American Ceramic Society

CREEP AND DENSIFICATION DURING SINTERING OF GLASS POWDER COMPACTS

M.N. Rahaman, L.C. De Jonghe,
G.W. Scherer, and R.J. Brook

March 1987

TWO-WEEK LOAN COPY

This is a Library Circulating Copy which may be borrowed for two weeks.

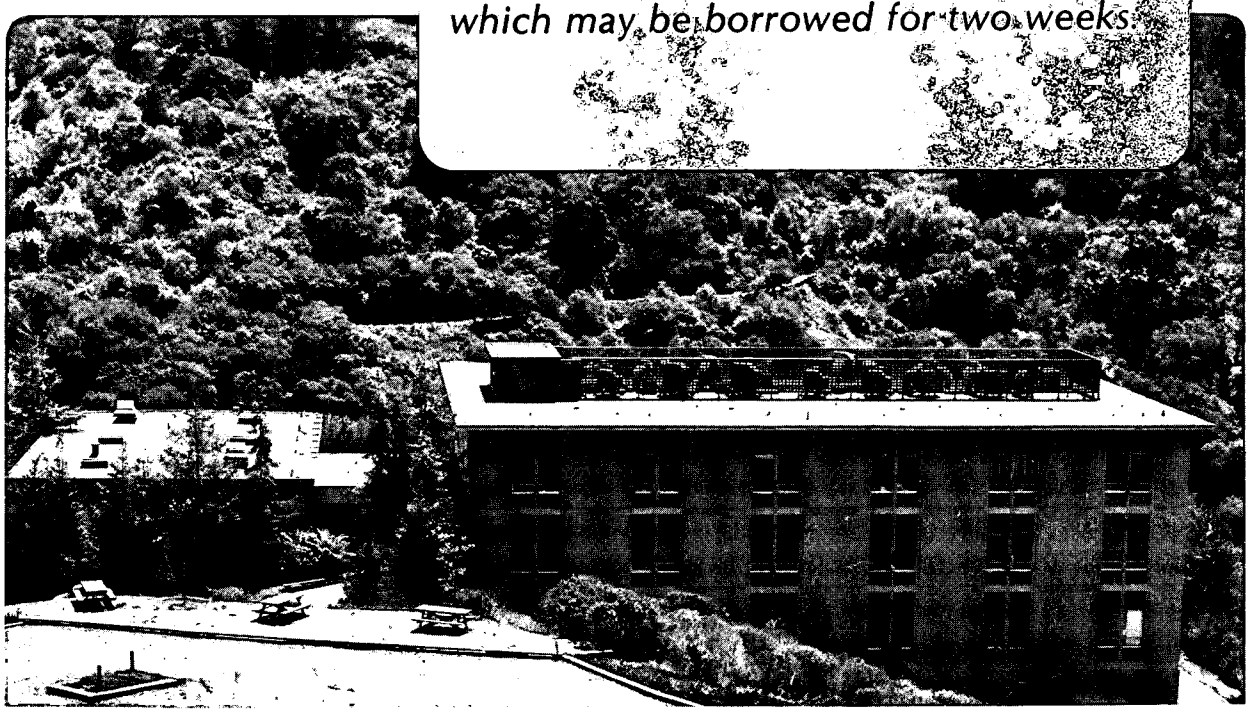

LBL-23177 c.2

Prepared for the U.S. Department of Energy under Contract DE-AC03-76SF00098

DISCLAIMER

This document was prepared as an account of work sponsored by the United States Government. While this document is believed to contain correct information, neither the United States Government nor any agency thereof, nor the Regents of the University of California, nor any of their employees, makes any warranty, express or implied, or assumes any legal responsibility for the accuracy, completeness, or usefulness of any information, apparatus, product, or process disclosed, or represents that its use would not infringe privately owned rights. Reference herein to any specific commercial product, process, or service by its trade name, trademark, manufacturer, or otherwise, does not necessarily constitute or imply its endorsement, recommendation, or favoring by the United States Government or any agency thereof, or the Regents of the University of California. The views and opinions of authors expressed herein do not necessarily state or reflect those of the United States Government or any agency thereof or the Regents of the University of California.

CREEP AND DENSIFICATION

DURING SINTERING OF GLASS POWDER COMPACTS

M.N. Rahaman[*+] and L.C. De Jonghe[*], Materials and Chemical Sciences Division, Lawrence Berkeley Laboratory, and University of California, Berkeley CA 94720

G.W. Scherer[*], Central Research and Development Department, Experimental Station 356/384, E.I. du Pont de Nemours and Co., Wilmington, DE 19898

R.J. Brook[*], Department of Ceramics, University of Leeds, Leeds LS2 9JT, England

ABSTRACT:

The simultaneous creep and densification of glass powder compacts was studied as a function of low applied uniaxial stress, temperature, and particle size. The creep rate can be expressed as the sum of the contribution from the applied stress that varies linearly with stress, and a contribution due to anisotropic densification that varies linearly with the densification rate. For a constant applied stress, the ratio of the creep rate to the densification rate is almost independent of both temperature and density. While these observations are consistent with the model of Scherer for the viscous sintering of glass, other observations show significant deviations from the model. Both the densification rate and the creep viscosity, which has an exponential dependence on porosity, show much stronger dependence on density compared with theoretical predictions.

Presented in part at the 88th Annual Meeting of the American Ceramic Society, Chicago, IL, April 28, 1986 (Paper 69-B-86).

[+]Present Address: The University of Missouri-Rolla, Ceramic Engineering Department, Rolla, MO 65401

[*]Member, The American Ceramic Society

Supported by the Division of Materials Science, Office of Basic Energy Sciences, U.S. Department of Energy, under Contract No. DE-AC03-76SF00098.

I. INTRODUCTION

The early work on the sintering of glass originated from the theory of viscous sintering by Frenkel.[1] Using a simple energy balance, i.e. that the energy dissipated by viscous flow is equal to the energy gained by the reduction of surface area during sintering, Frenkel derived equations for the neck growth between two glass spheres and for the shrinkage of a row of glass spheres. A numerical error in Frenkel's analysis was corrected by Eshelby.[2] The predictions of Frenkel's analysis have been supported by the experimental results of Kuczynski,[3] Kingery and Berg,[4] and Kuczynski and Zaplatynski.[5] Using Frenkel's energy balance concept, Mackenzie and Shuttleworth[6] developed a theory for the sintering of glass based on a simple model consisting of isolated, spherical pores of the same size in a dense matrix. Mackenzie and Shuttleworth's analysis is therefore strictly applicable to the final stage of sintering.

Experimentally, Culter and Hendricksen[7] have pointed out the effects of particle shape on the sintering of glass. They found that compacts of crushed, jagged particles sintered as much as 5 times faster than compacts of spheroidized particles of the same size. They attributed the faster sintering rates of crushed particles to the sharper radii at points of contact between the particles. Giess et al[8,9] have investigated the effects of particle shape on shrinkage anisotropy during sintering of cordierite-type glass powders. For jagged (ball-milled) and spheroidized powders uniaxially pressed into right cylinders, they found that both types of particle compacts exhibited about the same 0.7 anisotropy of the ratio of the axial to the radial shrinkage, but that spheroidizing reduced the shrinkage rate. Anisotropic shrinkage appears to be not a simple particle shape effect but may be related to particle packing and size distribution in the axial and radial directions.

Using Frenkel's energy balance concept, Scherer[10-12] considered a model that applies to the entire densification process but assumed a particular geometry consisting of cylinders connected into a cubic array. This model may not resemble the microstructure of an actual powder compact but it is believed to provide a reasonable representation of the structures of such materials as flame oxidation performs,[10] phase-separated and leached glasses,[11,15] and inorganic gels.[16] In spite of the geometry of the model, the predicted sintering kinetics agree very well with the predictions of Frenkel's analysis[1] for neck growth between spheres, and with Mackenzie and Shuttleworth's analysis[6] for the sintering of closed, isolated pores. Scherer's model appears therefore to have broad applicability. The model has also been applied to the sintering of a body with a bimodal pore size distribution,[13] to the sintering of a porous glass layer on a rigid substrate,[14] and to the sintering of glass subjected to applied stress.[17,18] Recently, Rabinovich[19] has compiled a review of the sintering of glass.

The effect of small, controlled uniaxial stress on the sintering behavior of glass powder compacts has not been investigated experimentally before. This paper seeks to address this problem. It describes the simultaneous creep and densification behavior during the sintering of glass powder compacts using the loading dilatometer technique[20] in which a small, measured uniaxial stress is applied to the sintering compact. The dependence of the creep rate and densification rate on applied stress, temperature, and particle size is explored. In addition to providing a better understanding of sintering and creep phenomena in glass, this work will also be relevant to glass systems in which transient stresses develop during sintering, such as multilayer ceramics and composites. Two of the

present authors have previously developed and applied the loading dilatometer technique to the sintering of polycrystalline oxides,[21-23] in which matter transport occurs by diffusion.

II. EXPERIMENTAL PROCEDURE

A commercial soda-lime glass powder* was used in this work. The powder was first air-classified to obtain narrow size fractions and these were examinined using a scanning electron microscope to determine their average particle sizes. These size fractions, denoted A, B and C were then selected and their average particle sizes were determined more accurately by counting the length intercepted by about 200 particles. The average particle sizes of A, B and C were 4μm, 8.5μm, and 33μm, respectively.

Carbowax** (8 vol%) was used as a binder in the compaction of the powder, since samples pressed without a binder were too weak for the sintering experiments. The carbowax was dissolved in chloroform, then the required amount of glass powder was dispersed in the solution, and the mixture was stir-dried. The powder was lightly ground in an agate mortar and pestle and uniaxially pressed at ~20 MPa into cylindrical compacts (6mm diameter by 6mm) with relative green densities of 0.55 ± 0.01.

Compacts were sintered in air for ~2 to 3 hours in a loading dilatometer.[20] Loads can be held constant to within ±0.5% for the duration of the experiment. Typically, the sample was placed in position between the pushrods of the dilatometer and then introduced into the outer zone of the furnace to allow burnout of the binder. The binder was removed by increasing the temperature of the sample by 50°C every 10 minutes up to

* Owens-Illinois, Perrysburg, OH 43551

**Union Carbide Corporation, New York, NY 10017

~350°C. After 30 min at this temperature, the sample was quickly introduced into the hot zone of the furnace. The load on the compact was applied rapidly and the axial shrinkage and temperature were recorded continuously. The mass and dimensions of the compacts were measured before and after they were sintered, and the final densities were measured using Archimedes' principle. In a separate set of experiments, sintering was terminated after times between 0 and 3 hours. The dimensions of these compacts were measured using a micrometer and the fracture surfaces were examined using scanning electron microscopy.

Generally, powder A (4μm) was used to explore the effects of applied stress and temperature. To explore the effects of stress, experiments were performed at 605°C and under stress of 0 to 30 kPa, while to explore the effect of temperature, experiments were performed at 580°C and 605°C and subjected to a stress of 9 kPa. Powders A, B and C were used to investigate the affect of particle size at 605°C and under a stress of 9 kPa.

In the dilatometer, a spring was used to maintain contact between the pushrod and the sample, and this exerted an additional force on the sample. This spring force was measured as a function of distance moved by the pushrod by replacing the sample with a sensitive strain gage. It was required to measure this force in only one experiment, since the initial length of the sample varied by less than 1% and the dilatometer measuring devices could be kept in a single position, initially, for all experimental runs.

X-ray diffraction measurements were performed on the glass powder and on the sintered material. For these, the sintered compacts were crushed and ground into a fine powder using a mortar and pestle. CuK_a radiation was used at a scanning rate of 1° 2θ min^{-1}.

The density of the bulk glass was also measured. About 10g of glass powder was placed in a platinum boat and heated to 1300°C at a rate of ~15°C/min, in a nitrogen atmosphere. After ~20 min at this temperature, the sample was slowly cooled to room temperature. The glass sample was then removed and its density measured using Archimedes' principle.

III. DATA ANALYSIS

The creep and densification strains were measured using a methodology described by Raj.[24] According to Raj, the creep strain rate, $\dot{\varepsilon}_c$, and the densification rate, $\dot{\varepsilon}_\rho$, are given by the relations:

$$\dot{\varepsilon}_c = (2/3)(\dot{\varepsilon}_z - \dot{\varepsilon}_r) \qquad \ldots(1)$$

$$\dot{\varepsilon}_\rho = \dot{\rho}/\rho = -(\dot{\varepsilon}_z + 2\dot{\varepsilon}_r) \qquad \ldots(2)$$

where $\dot{\varepsilon}_z$ and $\dot{\varepsilon}_r$ are the axial and radial strain rates and ρ is the relative density. If the sintering compact is subjected to an applied, axial stress, σ_z, then the mean hydrostatic stress, σ_h, experienced by the compact is

$$\sigma_h = \sigma_z/3 + \Sigma \qquad \ldots(3)$$

where Σ is the sintering stress (pressure) due to reduction in surface area.

The experimental measurements provided data for the change in length and radius of the sample with time. These data were converted to true strains by using the definitions appropriate for large deformations. If L(t) and R(t) are the time dependent length and radius, respectively, of the sample then, ε_z and ε_r may be written as

$$\dot{\varepsilon}_z = \frac{d[\ln (L/L_0)]}{dt} \qquad \ldots(4)$$

and

$$\dot{\varepsilon}_r = \frac{d[\ln(R/R_0)]}{dt} \qquad \ldots(5)$$

where L_0 and R_0 are the initial length and radius, respectively.

In each experiment the applied load on the sample consisted of two parts: a constant load, P, due to an electromagnetic loading device, and a load, S, due to the dilatometer spring that is required to maintain contact between the pushrod and the sample. The load S decreased approximately linearly with shrinkage of the sample and may be expressed as

$$S = S_0\ (1 - C\Delta L/L_0) \qquad \ldots(6)$$

where S_0 and C are constants derived experimentally and $\Delta L = L_0 - L$.

The cross-sectional area, A, of the sample changed with time, and is given by $A=\pi R^2$. Using equation (5) then

$$A = A_o \exp(2\varepsilon_r) \qquad \ldots(7)$$

where A_o is the initial cross-sectional area of the sample given by $A_o=\pi R_o^{\ 2}$.

Now the axial stress on the sample is given by

$$\sigma_z = (P + S)/A \qquad \ldots(8)$$

In these experiments, since A decreased with time, the decrease in S had a beneficial effect in reducing the magnitude of the change in σ_z with time. Using equations (6)-(8),

$$\sigma_z = [P + S_o(1-C+C\exp(\varepsilon_z))]/A_o\exp(2\varepsilon_r) \qquad \ldots(9)$$

IV. RESULTS

The X-ray diffraction results showed no traces of crystallinity in the samples before or after sintering. The complications of any amorphous to crystalline phase changes can therefore be eliminated from this work. The density of the bulk glass obtained by melting the glass powder was 2.43 ± 0.01 Mgm^{-3}, and this figure will be used as the theoretical density. Friction between the pushrods and the sample led to a small deviation from

cylindrical geometry in a narrow region of the sample near its contact surfaces. The diameter near the contact surfaces was slightly larger than that along the rest of the sample. These deviations from cylindrical geometry were small in all experiments and decreased with increasing applied load. The difference between the diameter at the contact surfaces and the average diameter of the sample, obtained from the length of the sample and its density, was less than 3% at the end of any experiment. Frictional effects between the pushrods and the sample are therefore relatively insignificant. Figure 1 shows the results for the load, S, due to the dilatometer spring vs axial shrinkage, $\Delta L/L_0$. The magnitude of S decreases from -0.12 N to zero for a sample shrinkage of 0.35.

Binder burnout was followed by having the dilatometer pushrod in contact with the sample, using the spring load only. The shrinkage of the sample (~2%) occured smoothly and was consistent with the value expected from the binder content (~8%). The amount of binder removed from the compact was ~95% of the value obtained from experiments on the loose powder.

The effects of applied stress, temperature, and particle size are now discussed separately in the following sections.

IV.(a) Effect of Applied Stress

Experiments were carried out on glass sample A, having an average particle size of 4μm and at 605°C under a total load (P + S) as outlined earlier. Figure 2 shows the axial strain, ε_z, versus time for values of P between 0 and 0.75N. A load of 1N on the sample represents a stress of 35 kPa on the green, unsintered compact and t = 0 represents the beginning of shrinkage. The load was applied quickly at t = 0 and the sintering temperature was reached after t = 8 min. Each curve is the average of two

runs under the same conditions and each is reproducible to within ±2%. It is seen that at any time, t, the axial strain increases with increasing load.

Figure 3 shows the results for ε_z vs the radial strain, ε_r, determined by sintering for times between 0 and 2.5 hours. Each experimental point was obtained using a different sample, and the binder burnout and experimental procedure for each was the same.

At low loads, ε_z is approximately proportional to ε_r, but above loads of ~(S + 0.25)N, the curves are slightly concave downwards. The curve denoted "0" is for a sample sintered without a spring load, i.e. the dilatometer pushrod was very near but not in contact with the sample. This sample shows a small amount of anisotropic densification, and the anisotropy ratio $k = (\varepsilon_z/\varepsilon_r) = 1.28$.

The results for ε_c and ε_ρ were obtained from Figures 2 and 3 and equations (1) and (2). A least squares technique was used to fit smooth curves through the results of Fig. 3, then at any t, both ε_z and ε_r were obtained. Figure 4 shows the results for ε_c vs t for three loads used. The densification strain was converted to relative density, ρ, and the results for ρ vs t are shown in Fig 5. It is seen that the applied loads caused extensive creep but had almost no effect on the densification. A small increase in density was observed, as shown in Fig 5, but the magnitude of this increase was within the limits of experimental error. The final value of $\rho = 0.95$ calculated from the shrinkage kinetics was within ~2% of the value found using Archimedes' principle. The negligible effect of applied load on the densification process can be understood from equation (3), if $\sigma_z/3$ is less than ~5% of Σ. Assuming the surface tension of the glass is ~0.3 Nm^{-1} and a mean pore radius of ~G/3, where G is the

particle size (~4 μm) then Σ ~-200 kPa, while the maximum value of $\sigma_z/3$ is ~-10kPa.

Since σ_z has a significant effect on ε_c, it is interesting to plot σ_z as a function of time (or density), using equation (9). From Fig 6 it is seen that σ_z is nearly constant (to within ~2%), and this results from the counterbalancing effect of the changes in the spring load, S, and the cross-sectional area, A.

By fitting smooth curves to the results of Fig 4 and 5, and differentiating, the relative densification rate, $\dot{\rho}/\rho$, and the creep rate, $\dot{\varepsilon}_c$, were obtained as a function of ρ (or t). For rigorous analysis of the data it is required to have results for $\dot{\rho}/\rho$, and $\dot{\varepsilon}_c$, vs ρ at a constant value of σ_z. Since Fig 6 indicates that σ_z is indeed nearly constant, no correction was necessary for these experiments. Figure 7 shows the results for $\dot{\rho}/\rho$ and $\dot{\varepsilon}_c$ vs ρ. The results for $\dot{\rho}/\rho$ were evaluated for the sample under the applied load, S, and $\dot{\varepsilon}_c$ was evaluated at σ_z values of 9, 18, and 27 kPa. The value of $\dot{\varepsilon}_c$ increases by a factor of ~2 between σ_z values of 9 and 27 kPa, while the effect of σ_z on ρ/ρ is negligible. The explanation for this is that $\dot{\varepsilon}_c$ is linearly dependent on σ_z, while $\dot{\rho}/\rho$ depends on $(\sigma_z/3 + \Sigma)$. If $\sigma_z \ll \Sigma$ then the effect of σ_z on $\dot{\rho}/\rho$ is negligible.

IV.(b) Effect of Temperature

The experiments were carried out at 605°C and 580°C, using the glass powder sample, A (~4 μm) and a load of (S + 0.25)N, where S is the spring load. Figure 8 show the results for the axial strain, ε_z, vs time, t. As for many glass systems, it is seen that a small change in temperature can lead to extensive changes in the shrinkage (or densification). The need for precise temperature control during studies on the sintering of glass is therefore emphasized.

The results for $\dot{\rho}/\rho$ and $\dot{\varepsilon}_c$ were calculated using the same procedure as that outlined in Section IV(a) above. Generally, $\dot{\rho}/\rho$ and $\dot{\varepsilon}_c$, at any ρ, increase with increasing temperature. This can be explained in terms of a decrease in the viscosities for densification and creep with increasing temperature. The most significant result is shown in Fig 9, where the ratio of $\dot{\varepsilon}_c$ to $\dot{\rho}/\rho$ is plotted vs ρ at 580°C and 605°C. It is seen that this ratio is almost independent of temperature and density. The constant value of $\dot{\varepsilon}_c/(\dot{\rho}/\rho)$ indicates that both the creep process and the densification process have the same temperature activation energy. Such a finding is quite plausible since both creep and densification occur by the same mechanism of viscous flow.

It is worth noting the contrasting effects of uniaxial (or shear) stress and temperature on creep and densification in glass. The creep rate, $\dot{\varepsilon}_c$, is found to be linearly dependent on σ_z, while $\dot{\rho}/\rho$ depends on the mean hydrostatic stress $(\sigma_z/3 + \Sigma)$, where Σ is the sintering stress due to reduction in surface area. Thus, $\dot{\varepsilon}_c$ increases much faster with σ_z, compared to $\dot{\rho}/\rho$. On the other hand, temperature changes $\dot{\varepsilon}_c$ and $\dot{\rho}/\rho$ by the same amount, and cannot, therefore, be used to vary the ratio $\dot{\varepsilon}_c/(\dot{\rho}/\rho)$.

IV.(c) Effect of Particle Size

The experiments were carried out at 605°C and under a load of (S+0.25)N, where S is the spring load, using three powder fractions A, B, and C having average particle sizes of 4, 8.5, and 33 μm, respectively. Fig 10 shows micrographs of A, B, and C, and it is seen that the particles have angular shapes typical of crushed glass.

Figure 11 shows the results for the axial strain, ε_z, vs time, t, for samples A, B, and C. It is seen that at any t, the value of ε_z increases as the initial particle size, G, of the compact decreases. Figure 12 shows

the results for ε_z vs the radial shrinkage, ε_r. The ε_z values are approximately proportional to ε_r and the slopes of the lines increase with increasing G.

The creep rate, $\dot{\varepsilon}_c$, and the densification rate, $\dot{\rho}/\rho$ were calculated using the procedure outlined in Section IV(a). Figure 13 shows the results for $\dot{\varepsilon}_c$ and $\dot{\rho}/\rho$ vs ρ for samples A, B, and C. The results for $\dot{\varepsilon}_c$ were evaluated at a constant stress, σ_z, equal to 9 kPa. It is seen that, at any ρ, both $\dot{\rho}/\rho$ and $\dot{\varepsilon}_c$ increase as the particle size, G, decreases. In addition the curves for $\dot{\rho}/\rho$ and $\dot{\varepsilon}_c$ appear to have similar shapes.

V. DISCUSSION

It is instructive to compare the experimental results of this study with the predictions of models for viscous sintering of glass. The analysis of Scherer[17] appears to be well suited to this comparison. The model[10] assumed a particular geometry, consisting of cylinders arranged in a cubic array. Sintering occurs as the cylinders reduce their surface area, becoming shorter and thicker.

The low stresses used in these experiments have almost no effect on the densification behavior of the sample. According to Scherer's analysis, the densification rate (under no externally applied load) is given by

$$\dot{\rho}/\rho = (k/\eta)[(3\pi)^{1/3}/2]\frac{(2-3cx)}{(x^{1/3}(1-cx)^{2/3})} \qquad \ldots(10)$$

where η is the viscosity of the bulk glass, c is a constant equal to $8\sqrt{2}/3\pi$, x is equal to a/l where a is the radius and l is the length of the cylinders of the model unit cell, and k is a constant given by

$$k = \gamma/(l_0\rho_0^{1/3}) \qquad \ldots(11)$$

In equation (11), γ is the surface tension of the glass, and l_0 and ρ_0 are the initial length and relative density, respectivley, of the unit cell.

In figure 14, the results for $\dot{\rho}/\rho$ for sample A sintered at 605°C (see Fig 7) are compared with the predictions of equation (10). The constant, $k(3\pi)^{1/3}/2\eta$, was arbitrarily chosen to give agreement between theory and experiment at $\rho = 0.8$. It is seen that the variation of $\dot{\rho}/\rho$ far exceeds the prediction of Sherer's model. The deviation between theory and experiment is not due to the binder burnout process, since a number of samples compacted without binder (and handled very genlty) showed similar densification behavior. One factor which may give rise to this deviation is the presence of a wide pore size distribution in the samples. As shown by Scherer,[13] the slope of $\dot{\rho}/\rho$ is sensitive to the pore size distribution. A mixture of pore sizes causes densification to be initially faster and finally slower than the unimodal case. Although mercury penetration porosimetry data are not available for the samples, the micrograph shown in Fig 15 for a compact sintered to a relative density of 0.8 does indeed indicate a distribution in pore sizes. Figure 15 also indicates that the pore morphology is strongly lenticular, and this may also contribute to the deviation between theory and experiment. The pore morphologies assumed in Scherer's model[10] and in the Mackenzie and Shuttleworth model[6] are drastically different from that of Fig 15.

For the creep data, the functional dependence of $\dot{\varepsilon}_c$ on σ_z may be explored by replotting the data of Fig 7 as $\dot{\varepsilon}_c$ vs σ_z at different values of ρ. This is shown in Fig 16. It is seen that $\dot{\varepsilon}_c$ increases linearly with σ_z, in agreement with predicted stress dependence for a Newtonian viscous flow mechanism. An interesting aspect of the creep data is that they extrapolate to a significant value at $\sigma_z = 0$. This extrapolated creep

rate, $\dot{\varepsilon}_a$, depends on the compact density. In fact, if $\dot{\varepsilon}_a$ is plotted versus the relative densification rate, $\dot{\rho}/\rho$, an approximately linear relationship is evident, Fig 17. Thus at any ρ, the observed creep rate can be written as

$$\dot{\varepsilon}_c = \dot{\varepsilon}_a + \dot{\varepsilon}_\sigma \qquad \ldots(12)$$

where $\dot{\varepsilon}_\sigma$ represents the contribution from the applied stress σ_z. Equation (12) can also be written as

$$\dot{\varepsilon}_c = D\dot{\rho}/\rho + \sigma_z/\eta^* \qquad \ldots(13)$$

where D is a constant equal to 1/7, and η^* is the effective creep viscosity at density ρ.

A source of the extrapolated creep rate term, $\dot{\varepsilon}_a$, is anisotropic densification due to non-uniformity in the compact microstructure. As seen in Fig 3, the sample sintered under zero load (curve 0), shrinks somewhat faster in the axial direction, with $k = \varepsilon_z/\varepsilon_r = 1.28$. According to Scherer,[17] the axial strain rate of the sample is

$$\dot{\varepsilon}_z = \dot{\varepsilon}_{fz} + \sigma_z/F \qquad \ldots(14)$$

and the radial strain rate is

$$\dot{\varepsilon}_r = \varepsilon_{fr} - N\sigma_z/F \qquad \ldots(15)$$

where $\dot{\varepsilon}_{fz}$ and $\dot{\varepsilon}_{fr}$ are the "free" strain rates in the axial and radial directions for a sample under zero load. The function F is the resistance to flow (or "effective modulus"), given by

$$F = 3\eta\rho/(3-2\rho) \qquad \ldots(16)$$

where η is the viscosity of the bulk glass. The function N is the "effective Poisson's ratio", given by

$$N = 0.5\,[\rho/(3-2\rho)]^{1/2} \qquad \ldots(17)$$

The functions F and N should be tensors in an anisotropic body, but that refinement is omitted to simplify this discussion. The creep rate found from equation (1) due to Raj[24] can then be written as

$$\dot{\varepsilon}_c = (2/3)(\dot{\varepsilon}_{fz}-\dot{\varepsilon}_{fr}) + (2/3)(1+N)\sigma_z/F \qquad ...(18)$$

The creep rate found from Raj's method is seen to include a contribution from anisotropic densification of the sample. Equation (18) is similar to the experimentally derived relationships of the equations (12) or (13), with

$$\dot{\varepsilon}_a = (2/3)(\dot{\varepsilon}_{fz} - \dot{\varepsilon}_{fr}) \qquad ...(19)$$

and

$$\eta^* = 3F/[2(1+N)] \qquad ...(20)$$

The densification rate is, from equation (2)

$$\dot{\rho}/\rho = -(\dot{\varepsilon}_{fz}+2\dot{\varepsilon}_{fr}) - (1-2N)\sigma_z/F \qquad ...(21)$$

For the experiments of the study, the low applied stresses have almost no effect on densification as outlined earlier, so equation (21) may be written as

$$\dot{\rho}/\rho = -(\dot{\varepsilon}_{fz}+2\dot{\varepsilon}_{fr}) \qquad ...(22)$$

The slope of Fig 17 is given by equations (19) and (20)

$$\dot{\varepsilon}_a/(\dot{\rho}/\rho) = -(2/3)(\dot{\varepsilon}_{fz}-\dot{\varepsilon}_{fr})/(\dot{\varepsilon}_{fz}+2\dot{\varepsilon}_{fr}) \qquad ...(23)$$

Figure 3 suggests that

$$\varepsilon_{fz} \approx 1.8\varepsilon_{fr} \qquad ...(24)$$

for the sample sintered under zero load. Then from equation (23)

$$\dot{\varepsilon}_a/(\dot{\rho}/\rho) = -0.14 \qquad ...(25)$$

From Fig 17, the experimental value of this ratio is -0.14 in excellent agreement with equation (25). Thus Fig 17 follows directly from Figures 2 and 3 and this is consistent with Scherer's model.

From equations (18), (22), and (24), the ratio $\dot{\varepsilon}_c/(\dot{\rho}/\rho)$ plotted in Fig 9 is

$$\frac{\dot{\varepsilon}_c}{\dot{\rho}/\rho} \quad \frac{(2/3)(k-1)\dot{\varepsilon}_{fr} + (2/3)(1+N)\sigma_z/F}{(2+k)\dot{\varepsilon}_{fr}} \qquad \ldots(26)$$

This ratio is constant, since[17]

$$F\dot{\varepsilon}_{fr}/(1+N) = \text{constant} \qquad \ldots(27)$$

The quantity plotted in equation (26) is expected to be independent of temperature since $\dot{\varepsilon}_{fr}$ and 1/F are both inversely proportional to viscosity.

The particle size dependence of $\dot{\rho}/\rho$ and $\dot{\varepsilon}_c$ shown on Figure 13 can now be explained. The densification rate at any ρ is proportional to the mean hydrostatic stress, σ_h, given in equation (3). Thus

$$\dot{\rho}/\rho = \text{constant}(\sigma_z/3 + \Sigma) \qquad \ldots(28)$$

since $\sigma_z/3 << \Sigma$, then

$$\dot{\rho}/\rho = \text{constant}(\Sigma) \qquad \ldots(29)$$

Since the quantity Σ is inversely proportional to the mean pore radius, r, which in turn varies as the scale of the system i.e. the particle size, G, of the powder, then $\dot{\rho}/\rho$ should be proportional to 1/G. This is indeed so, as shown in Fig 18, where $\dot{\rho}/\rho$ is plotted vs. G_o/G, where G_o = 33 μm. The small deviations in this figure at G/G_o = 1 might be due to the $\sigma_z/3$ term in equation (28).

According to theory, the creep rate should depend on the load-bearing fraction of the cross-sectional area and be independent of particle size for mass tranport by a viscous flow mechanism. The observed dependence of $\dot{\varepsilon}_c$ on G might be due to anisotropic densification. From Fig 17, it is seen that the extrapolated creep rate, $\dot{\varepsilon}_a$, due to anisotropic densification is given by

$$\dot{\varepsilon}_a = (\dot{\rho}/\rho)/7 \qquad \ldots(30)$$

Then from equation (12), the creep rate contribution, ε_σ due to the applied stress, σ_z, is

$$\dot{\varepsilon}_\sigma = \dot{\varepsilon}_c - (\dot{\rho}/\rho)/7 \qquad \ldots(31)$$

Figure 19 shows $\dot{\varepsilon}_\sigma$ vs 1/G at three values of ρ, assuming that equation (30) applies for all G. The curves for $\dot{\varepsilon}_\sigma$ are indeed independent of particle size.

The effective viscosity for creep, η^*, is defined from equations (12) and (13) as

$$\eta^* = \sigma_z/\dot{\varepsilon}_\sigma \qquad \ldots(32)$$

and its dependence on density can be calculated from the results of Fig 16. For σ_z = 9 kPa, the data for $\dot{\varepsilon}_\sigma$ are plotted vs porosity, P = $(1-\rho)$ as shown in Fig 20. The results show that η^* has a strong exponential dependence on P (or ρ) and can be expressed as

$$\eta^* = \eta \exp(-a_e P) \qquad \ldots(33)$$

where a_e = 11.2 ±0.02, and η is the viscosity of the bulk glass. The value of η found by extrapolating the data of Fig 20 to zero porosity is $(1.3\pm0.01)\times10^{10}$ $Nm^{-2}s$. The creep viscosity, η^*, can also be found from the data of Fig 19 and remarkably good agreement with the results of Fig 20 is found.

From equation (18) it is evident that according to Scherer's theory, η^* can be expressed as

$$\eta^* = 3F/2(1+N) \qquad \ldots(34)$$

The value of η^* was calculated as a function of ρ using equations (16) and (17), and the bulk viscosity, η, was arbitrarily chosen to give agreement with the experimental results ρ = 1. Figure 21 shows a comparison between the experimental and theoretical values for η^*/η plotted as a function of porosity. The difference is quite spectacular. Equation (34) may be

adequately approximated as

$$\eta^* \approx \eta \exp(-a_t P) \qquad \ldots(35)$$

where $a_t = 2.4$. The value of a_t is nearly 5 times lower than the experimentally derived value of 11.2. The difference between the two values may originate in the strongly lenticular shape of the pores in the present glass compacts, as evident in Fig. 15. Indeed, lenticular pores will tend to increase a_e. The lenticular pore shape may also have led to the other surprising feature of the results, namely the direction of the shrinkage anisotropy (Fig 3). Geiss et al[8,9] found that the shrinkage was less in the axial direction, which is the direction of pressing during preparation of the samples. However, the samples used in the present study showed the opposite behavior. It is likely that the pore orientation that caused that anisotropy may also allow greater compliance in the z-direction.

Further experimental work is in progress to determine whether the strong dependence of $\dot{\rho}/\rho$, and η^* on ρ is a general result and how these quantities depend on anisotropic densification, pore morphology, and pore size distribution.

VI. CONCLUSIONS

The loading dilatometer technique has been used to investigate the creep and densification behavior of glass powder compacts. This is the first time that the effect of small, controlled uniaxial (or shear) stresses on the sintering of glass has been systematically studied.

The creep rate can be expressed as the sum of a contribution from the applied stress that varied linearly with stress, and a contribution due to anisotropic densification that varied linearly with the densification rate. At a constant stress, the ratio of the creep rate to the densification rate

was found to be independent of both density and temperature. These observations are consistent with Scherer's model for the viscous sintering of glass.

The dependence of the densification rate, $\dot{\rho}/\rho$, and the creep viscosity, η^*, on density, however, showed very drastic deviation from Scherer's theory. The strong dependence of ρ/ρ on density may be due to the pore size distribution in the samples. The creep viscosity, η^*, was also found to have a strong dependence on porosity, P, and can be expressed by an equation of the form $\eta^* = \eta \exp(-11.2P)$, where η is the viscosity of bulk glass; according to Scherer's model, $\eta^* \sim \eta \exp(-2.4P)$. The difference is thought to result from the lenticular pore shape in the samples, which may also have caused the unstressed samples to shrink anisotropically. The bulk viscosity, η, was 1.3×10^{10} $Nm^{-2}s$.

REFERENCES

1. J. Frenkel, "Viscous Flow of Crystalline Bodies Under the Action of Surface Tension", J. Phys. (Moscow) 9 (5) 385-91 (1945).

2. J.D. Eshelby in Discussion of "Seminar on the Kinetics of Sintering" by A.J. Shaler, Metals Trans., 185 806, November 1949.

3. G.C. Kuzcynski, "Study of the Sintering of Glass" J. Appl. Phys. 20 (12) 1160-63 (1949).

4. W.D. Kingery and M. Berg, "Study of the Initial Stages of Sintering Solids by Viscous Flow, Evaporation-Condensation, and Self-Diffusion", J. Appl. Phys. 26 (10) 1205-12 (1955).

5. G.C. Kuzcynski and I. Zaplatynskyj, "Sintering of Glass", J. Amer. Ceram. Soc. 39 (10) 349-50 (1956).

6. J.K. Mackenzie and R. Shuttleworth, "A Phenomenological Theory of Sintering", Proc. Phys. Soc., London 62 (12B) 833-52 (1949).

7. I.B. Cutler and R.E. Hendricksen,"Effect of Particle Shape on the Kinetics of Sintering of Glass", J. Amer. Ceram. Soc. 51 (10) 604-5 (1968).

8. E.A. Giess, J.P. Fletcher, and L.W. Herron, "Isothermal Sintering of Cordierite - Type Glass Powders", J. Amer. Ceram. Soc., 67 (8) 549-52 (1984).

9. E.A. Giess, C.F. Guerci, G.F. Walker, and S.H. Wen, " Isothermal Sintering of Sheroidized Cordierite - Type Glass Powders", J. Amer. Ceram. Soc., 68 (12) C-328-29 (1985).

10. G.W. Scherer, "Sintering of Low-Density Glasses: I, Theory", J. Amer. Ceram. Soc. 60 (5-6) 239-43 (1977).

11. G.W. Scherer and D.L. Bachman, "Sintering of Low-Density Glasses: II, Experimental Study", J. Amer. Ceram. Soc. 60 (5-6) 239-43 (1977).

12. G.W. Scherer, "Sintering of Low-Density Glasses: III, Effect of a Distribution of Pore Sizes", J. Amer. Ceram. Soc. 60 (5-6) 239-43 (1977).

13. G.W. Scherer, "Viscous Sintering of a Bimodal Pore-Size Distribution", J. Amer. Ceram. Soc. 67 (11) 709-15 (1984).

14. G.W. Scherer and T. Garino, "Viscous Sintering of a Rigid Substrate", J. Amer. Ceram. Soc. 68 (4) 216-20 (1985).

15. G.W. Scherer and M.G. Drexhage, "Stress in Leached Phase-Separated Glass", J. Amer. Ceram. Soc. 68 (8) 419-26 (1985).

16. C.J. Brinker and G.W. Scherer, "Relationships Between the Sol-to-Gel and Gel-to-Glass Conversions", pp. 43-59 in Ultrastructure Processing of Ceramics, Glasses and Compositions. L.L. Hench and D.R. Ulrich (Ed:) Wiley, New York (1984)

17. G.W. Scherer, "Sintering Inhomogeneous Glasses: Application to Optical Wavelengths", J. Non-Cryst. Solids 34 239-56 (1979).

18. G.W. Scherer, "Viscous Sintering Under a Uniaxial Load", J. Amer. Ceram. Soc. 69 (9) C-206-7 (1986).

19. E.M. Rabinovich, "Preparation of Glass by Sintering", J. Mater. Sci., 20 (11) 4259-97 (1985).

20. L.C. De Jonghe and M.N. Rahaman, "A Loading Dilatometer", Rev. Sci. Instrum., 55 (12) 2007-10 (1984).

21. M.N. Rahaman and L.C. De Jonghe, "Sintering of CdO Under Load Applied Stress", J. Am. Ceram. Soc., 67 (10) C-205-7 (1984).

22. M.N. Rahaman, L.C. De Jonghe, and R.J. Brook, "Effect of Shear Stress on Sintering", J. Am. Ceram. Soc., 69 (1) 53-58 (1986).

23. M.N. Rahaman, L.C. De Jonghe, and C.H. Hsueh, "Creep During Sintering of Porous Compacts", 69 (1) 58-60 (1986).

24. R. Raj, "Separation of Cavitation Strain and Creep Strain During Deformation", J. Am. Ceram. Soc., 65 (3) C-46 (1982).

LIST OF FIGURES

Figure 1. The load applied to the sample by the dilatometer spring vs axial shrinkage of the sample. The spring load is required to maintain contact between the pushrod and the sample.

Figure 2. The axial strain vs time for glass powder fraction, A, sintered at 605°C under different applied axial loads (in newton). The quantity S represents the spring load of the dilatometer.

Figure 3. The axial strain vs the radial strain for the experiments described in Fig. 2. The curve labelled 'O' is for a sample sintered under zero load.

Figure 4. The creep strain vs time calculated from Figs. 2 and 3, and Eqn. (1).

Figure 5. The relative density vs time calculated from Figs. 2 and 3, and Eqn. (2).

Figure 6. The applied axial stress vs time for the loads used (shown in newton).

Figure 7. The creep rate and densification rate vs relative density for the constant axial stresses (shown in kPa). The densification rate was almost independent of these low stresses used.

Figure 8. The axial strain vs time for glass powder fraction, A, sintered under an axial load of (S+0.25)N at 580°C and 605°C.

Figure 9. The ratio of the creep rate to the densification rate vs relative density for the experiments described in Fig. 8.

Figure 10. Scanning electron micrographs of powder fractions A, B, and C having average particle sizes of 4, 8.5 and 33 μm, respectively.

Figure 11. The axial strain vs time for glass powder fractions A, B, and C sintered at 605°C and under an axial load of (S+0.25)N.

Figure 12. The axial strain vs the radial strain for the experiments described in Fig. 11.

Figure 13. The creep rate and the densification rate vs. relative density for the experiments described in Fig. 11 at a constant axial stress of 9 kPa.

Figure 14. Comparison of the experimental results for the densification rate vs. relative density with the predictions of Scherer's model given in Eqn. (10).

Figure 15. Pore microstructure of glass powder fraction, A, sintered at 605°C to a relative density of ~0.8. The axial load used was (S+0.25)N.

Figure 17. The extrapolated creep rate vs the densification rate using the data of Figs. 7 and 16.

Figure 18. The densification rate vs the inverse of the particle size of the glass powder plotted from the data of Fig. 13. G_o = 33μm.

Figure 19. The creep rate, due to an applied axial stress of 9 kPa, vs the inverse of the particle size of the glass powder plotted from the data of Fig. 13 and Eqn. (31). G_o = 33μm.

Figure 20. The creep rate due to an applied axial stress of 9 kPa, vs porosity, using the data of Fig. 16 and Fig. 19.

Figure 21. The ratio of the creep viscosity to the bulk viscosity of the glass found from the experimental results of Fig. 20 and compared with the predictions of Scherer's theory given by Eqn. (34).

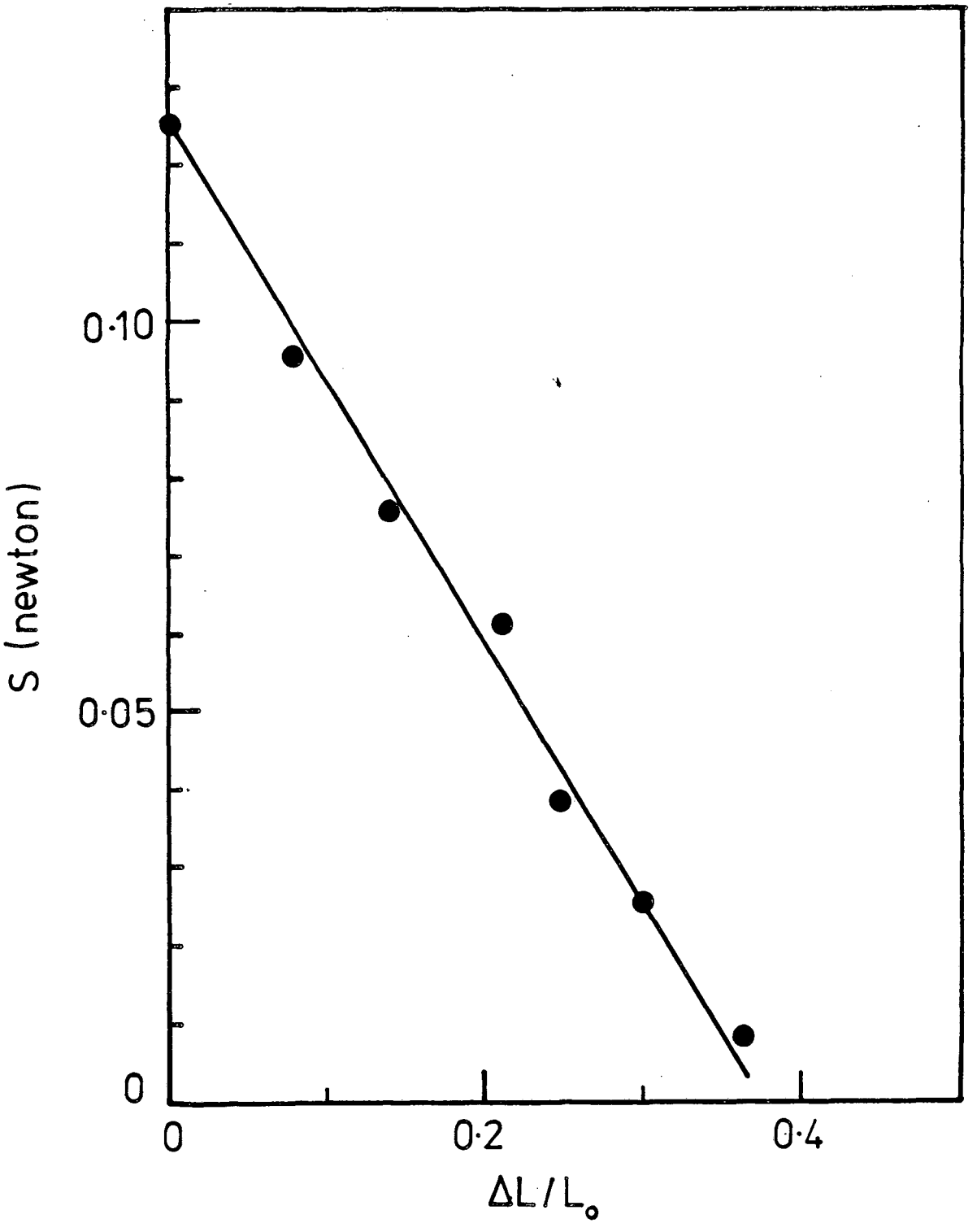

XBL 873-1013

Fig. 1

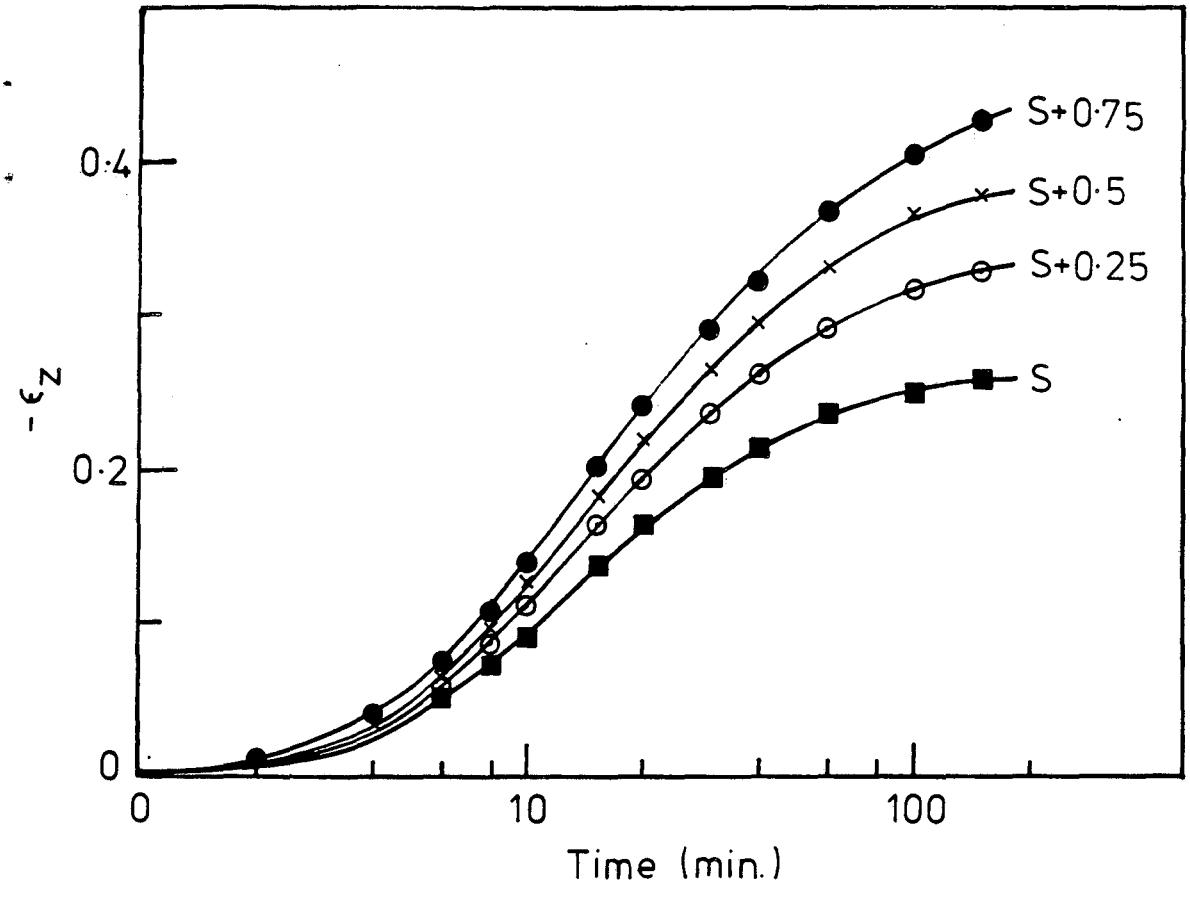

XBL 873-1012

Fig. 2

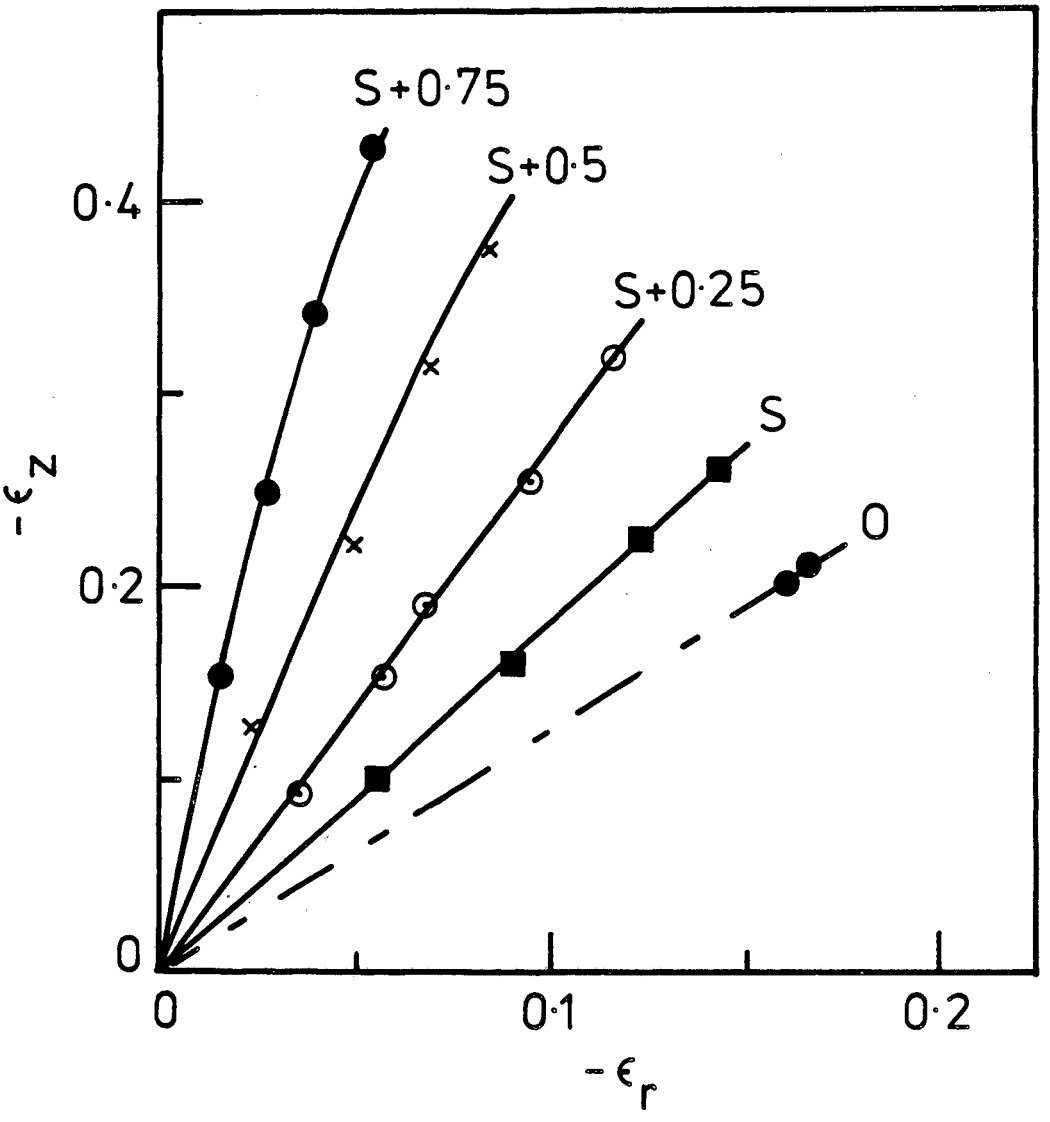

XBL 873-1011

Fig. 3

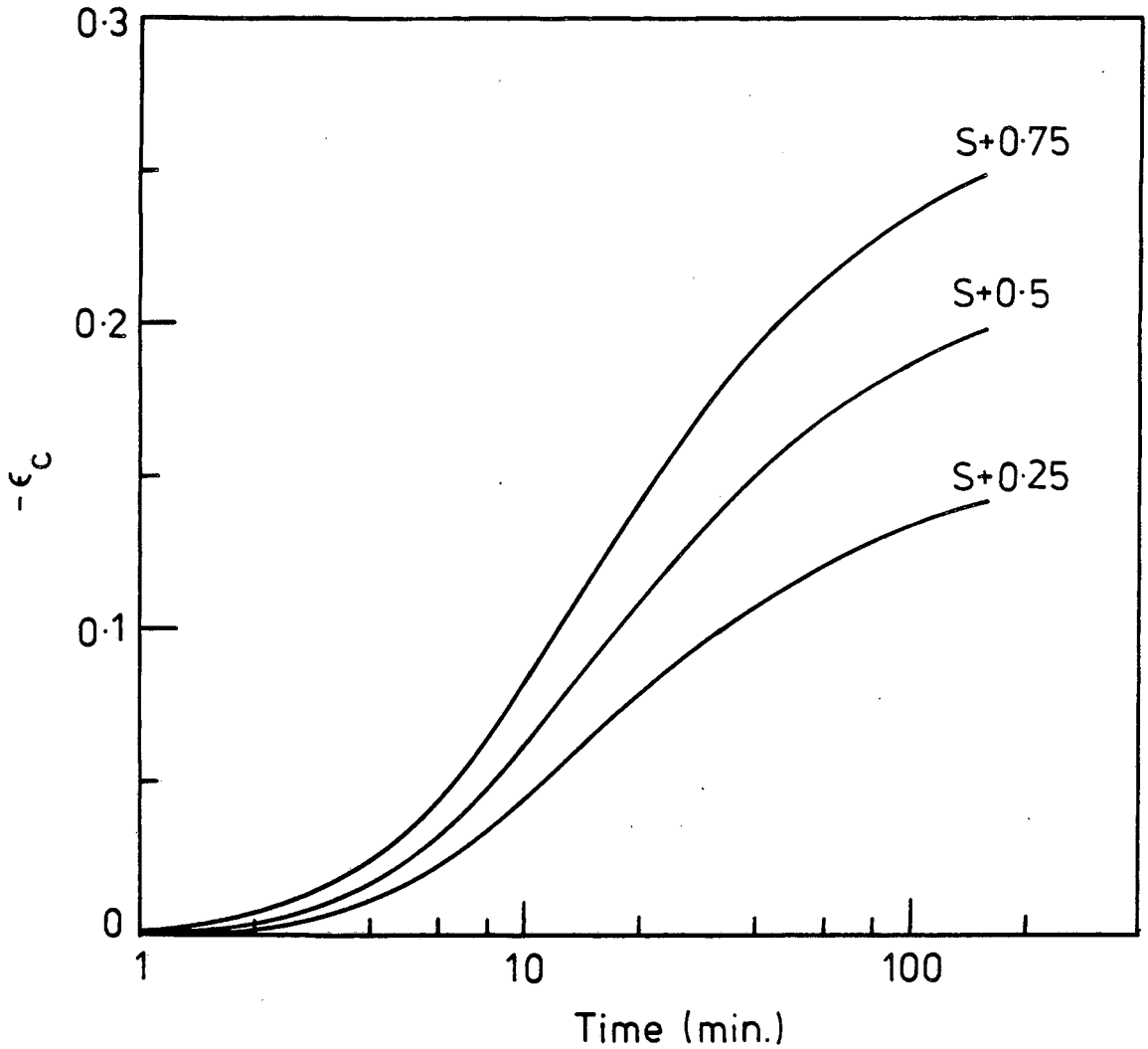

XBL 873-1010

Fig. 4

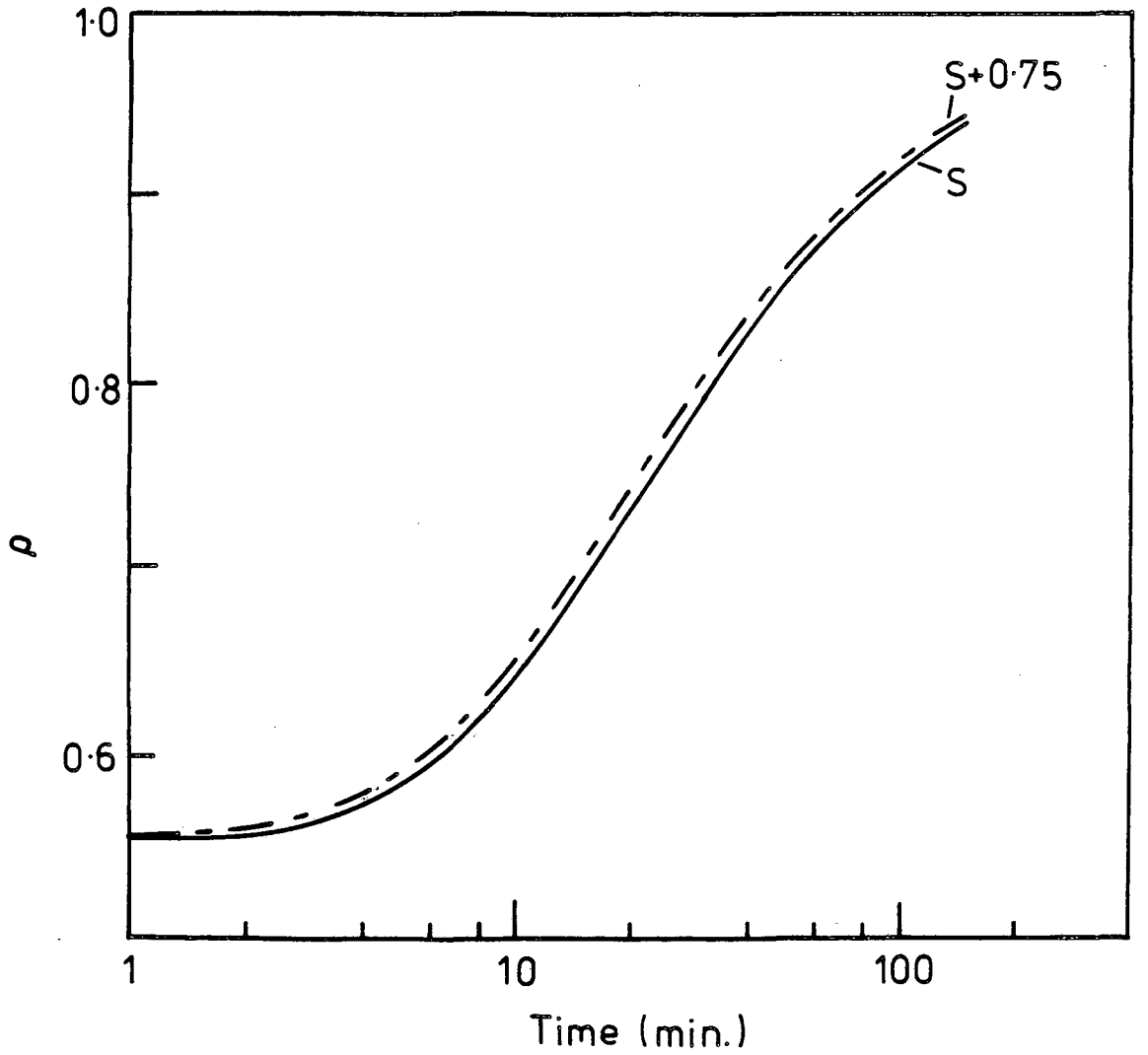

XBL 873-1009

Fig. 5

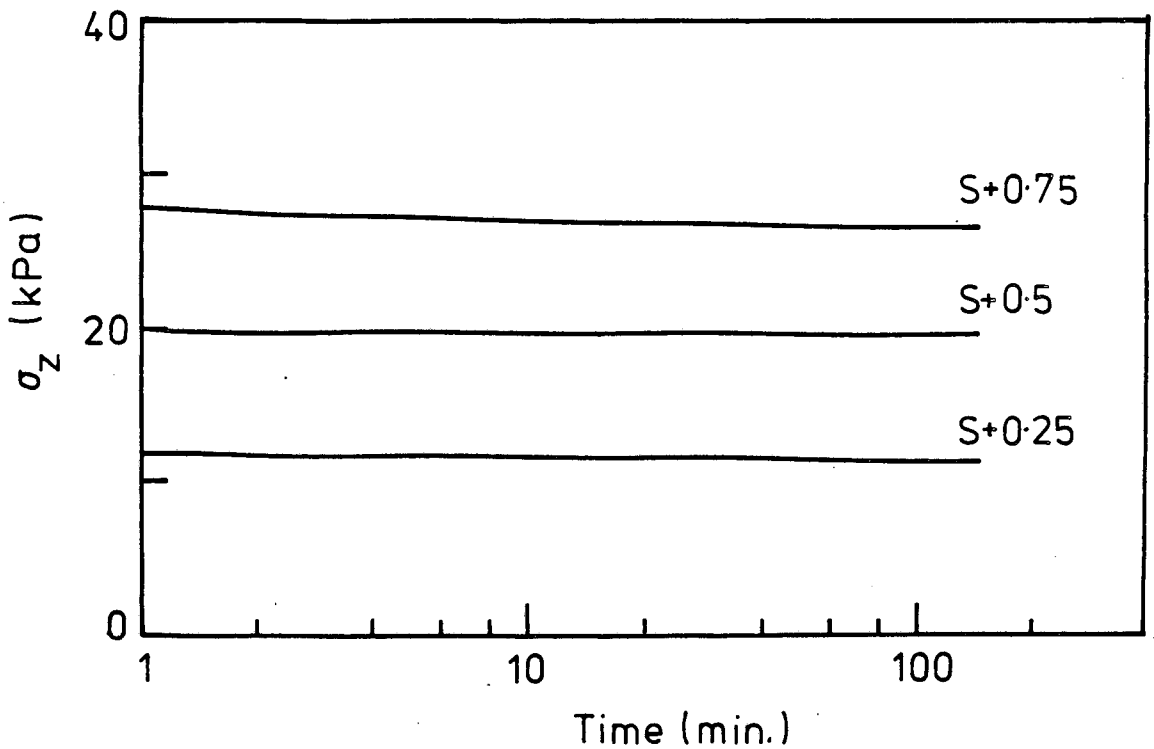

XBL 873-1008

Fig. 6

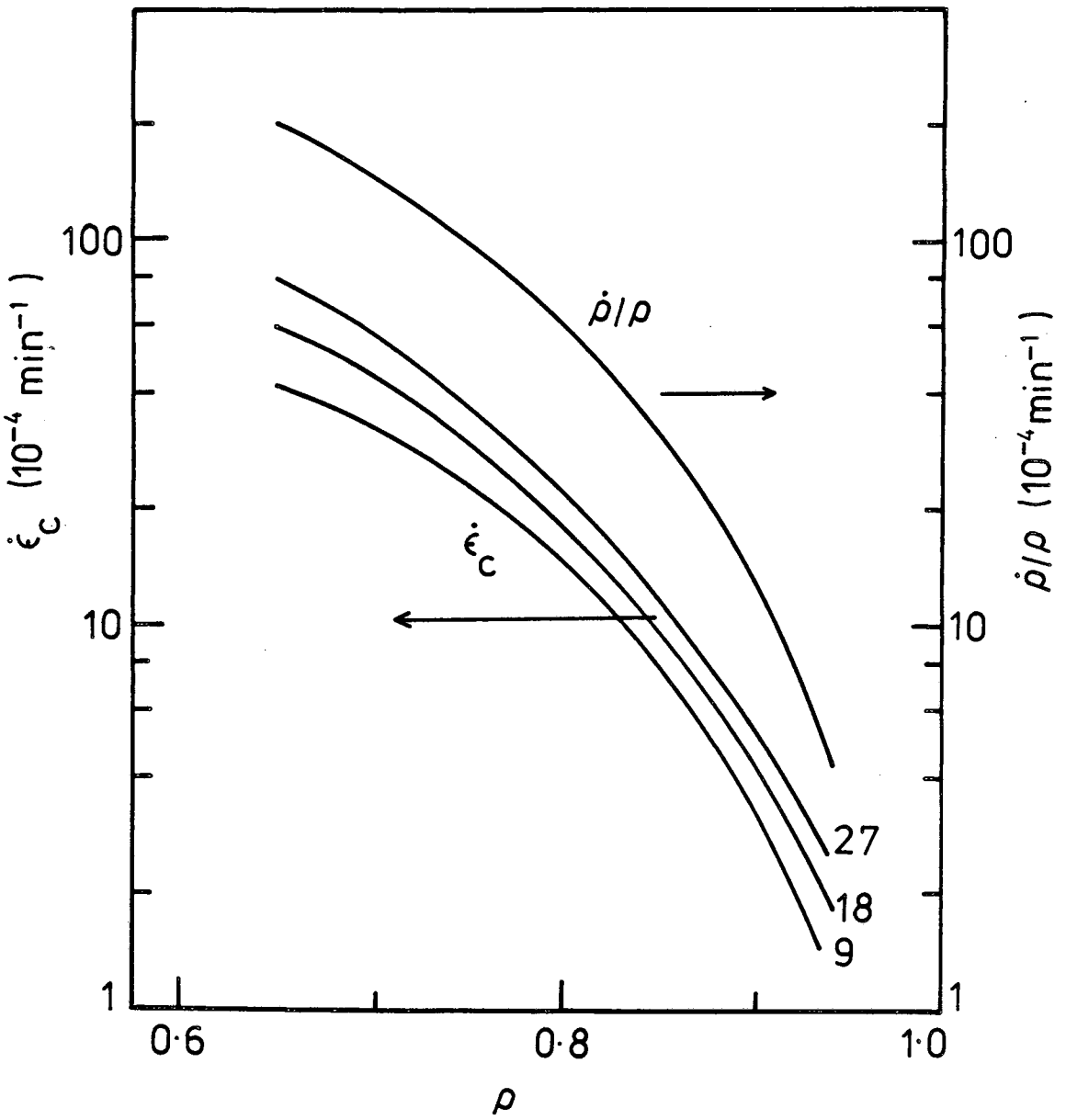

XBL 873-1007

Fig. 7

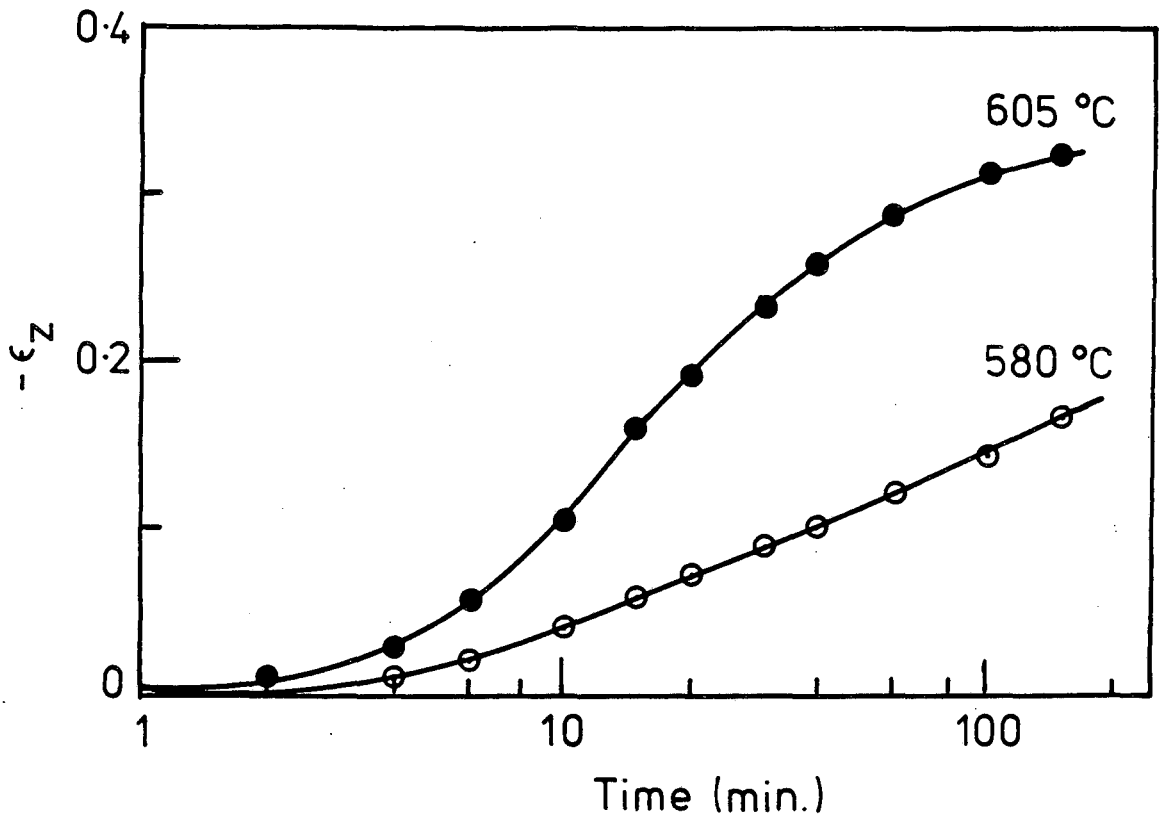

XBL 873-1006

Fig. 8

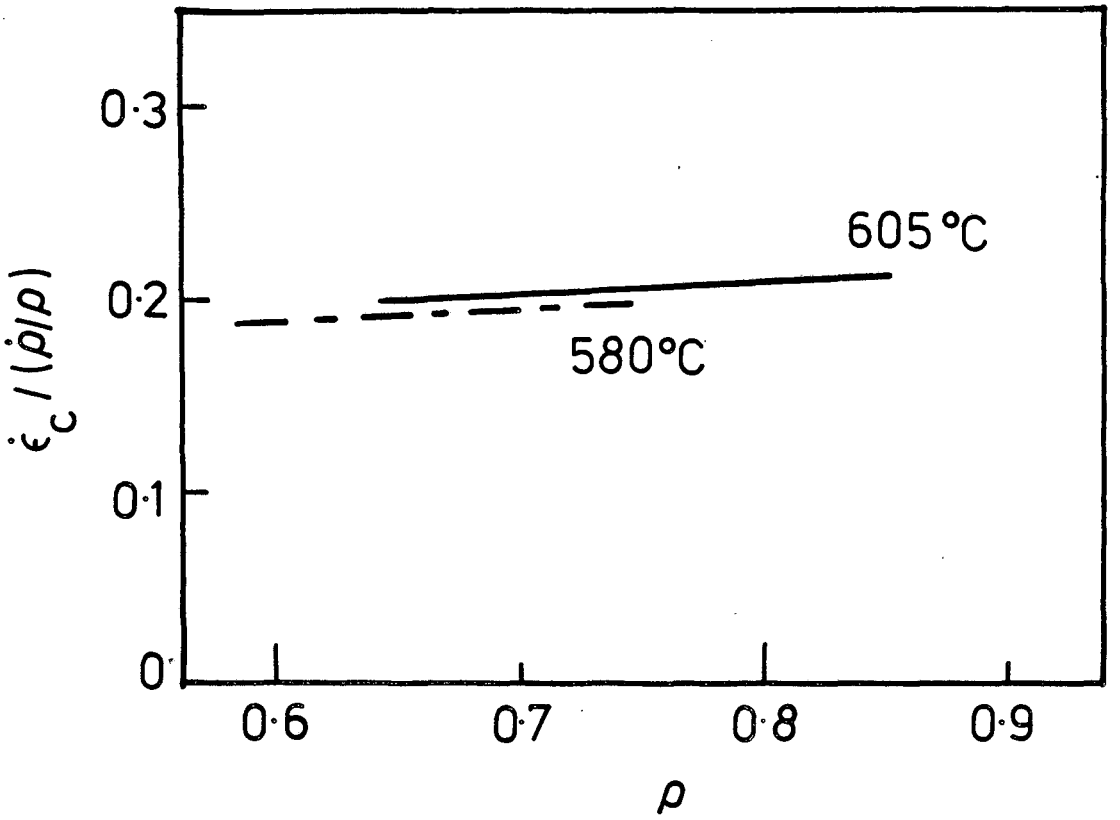

XBL 873-1005

Fig. 9

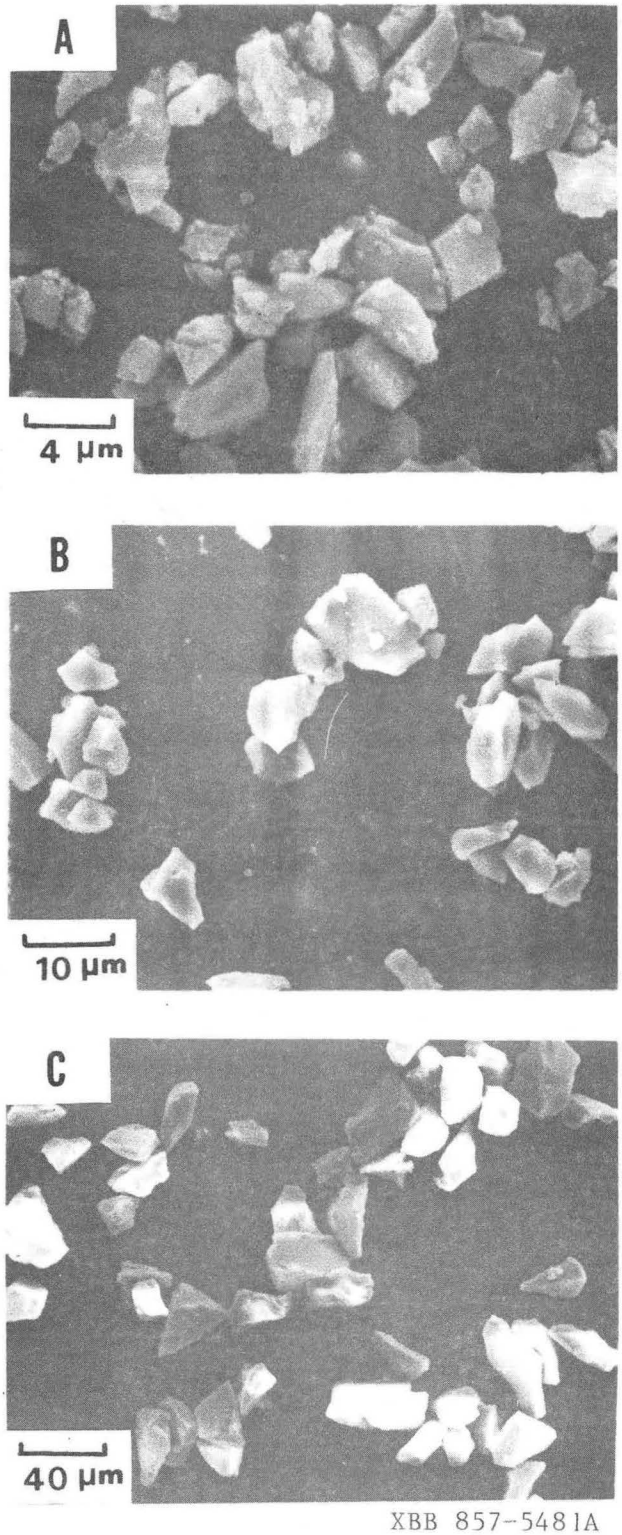

XBB 857-5481A

Fig. 10

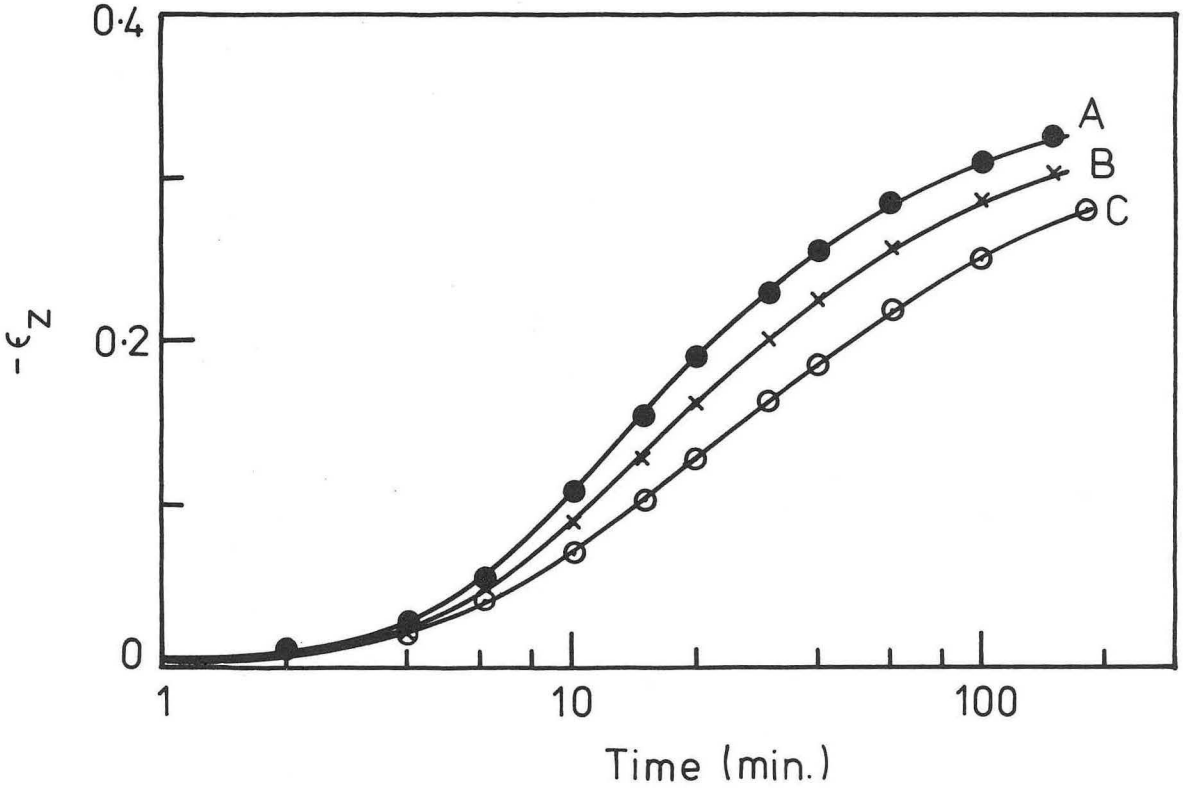

XBL 873-1014

Fig. 11

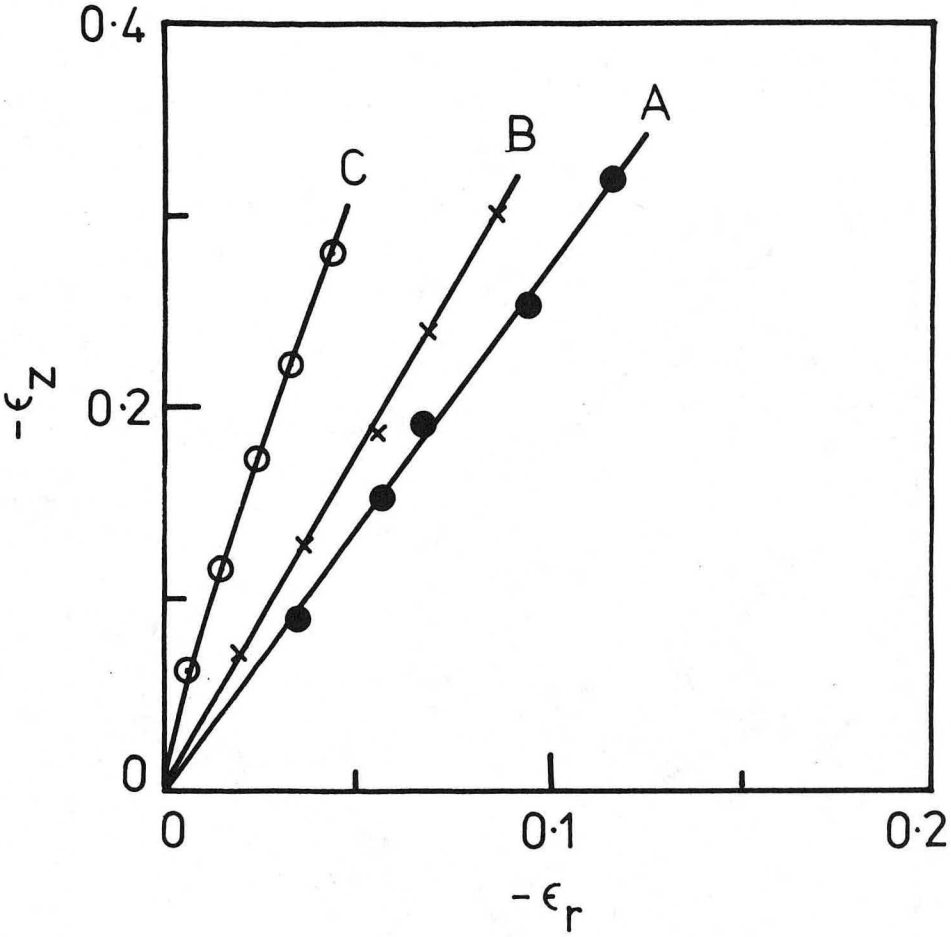

XBL 873-1015

Fig. 12

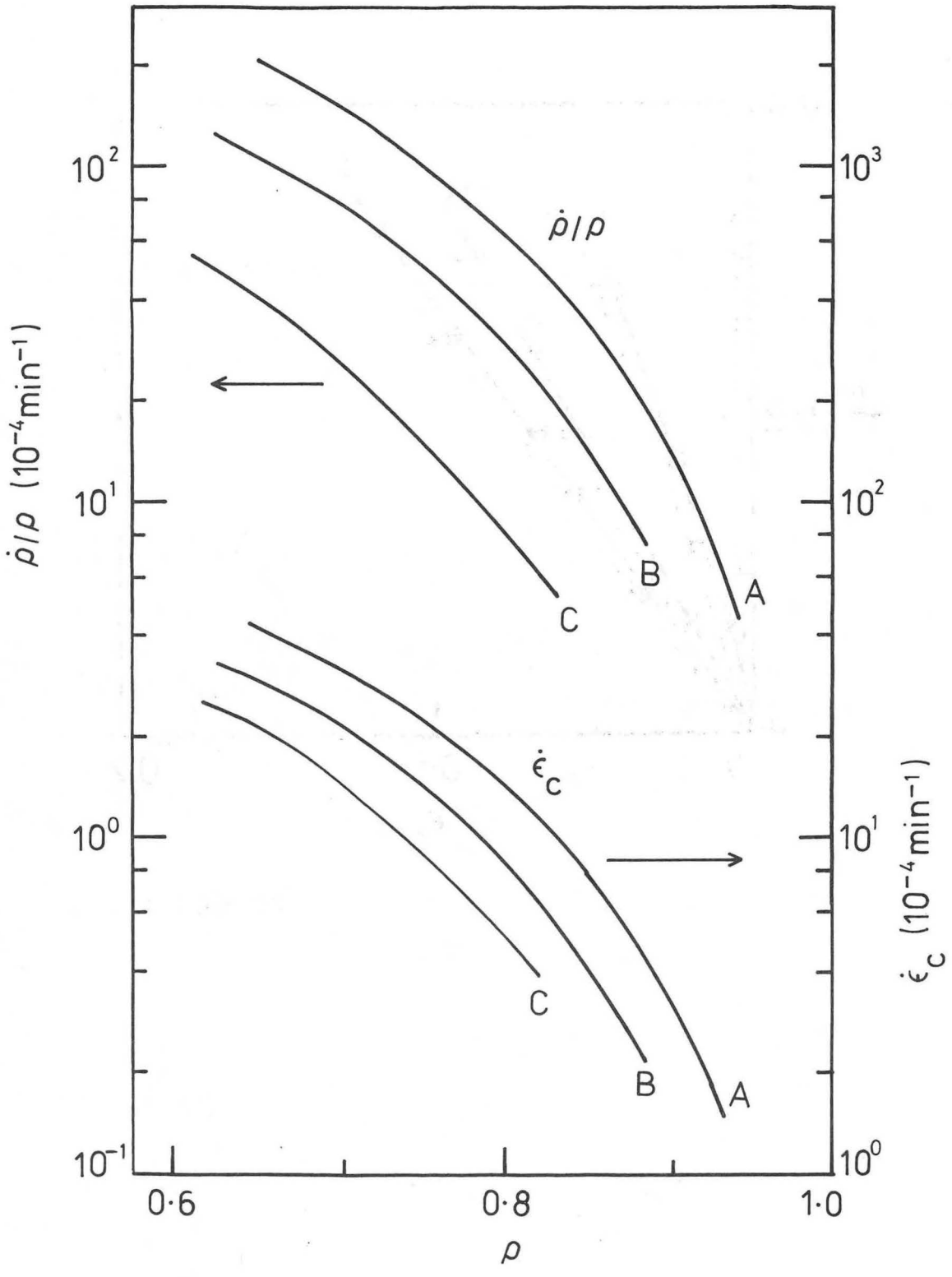

XBL 873-1016

Fig. 13

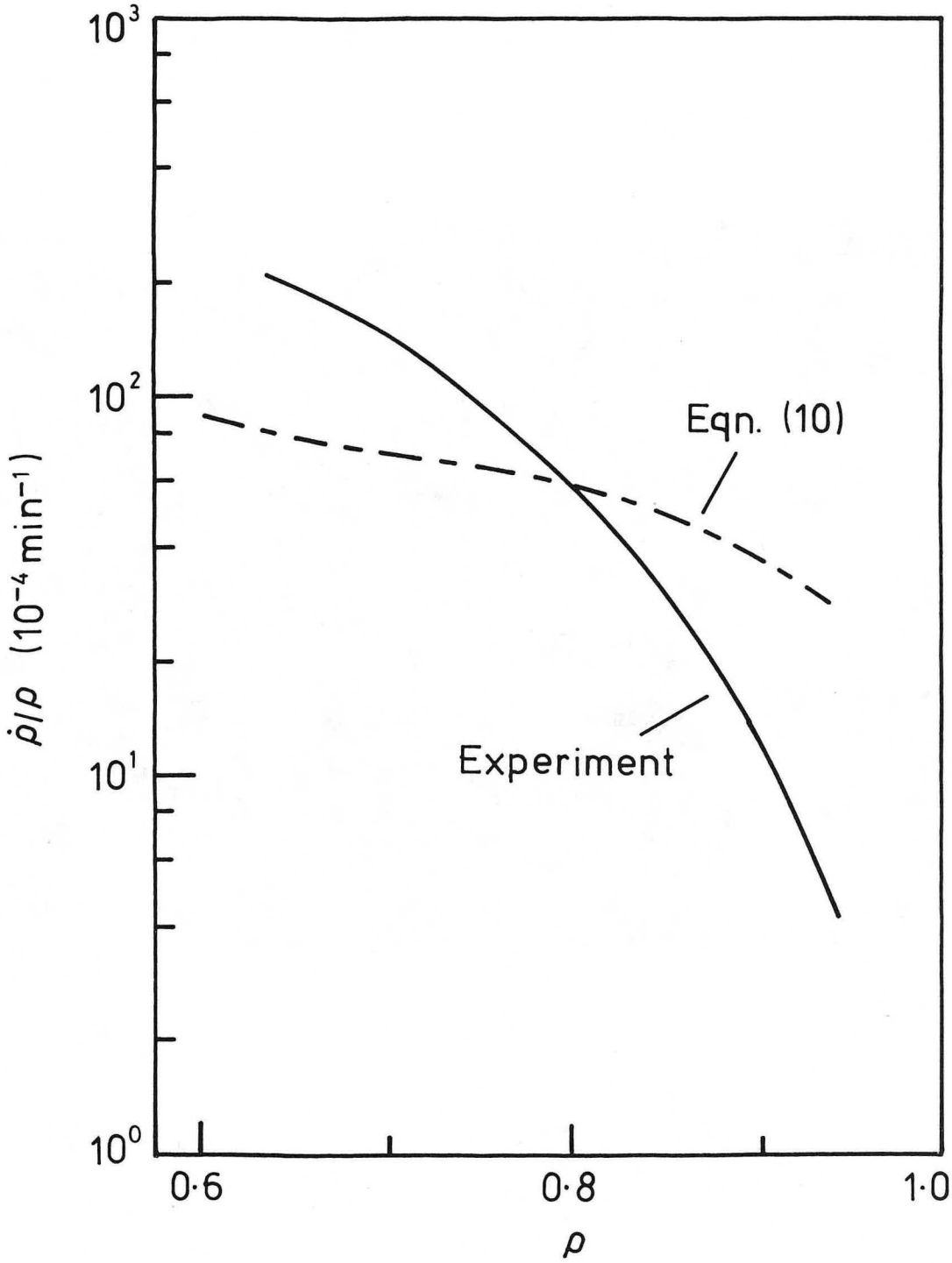

XBL 873-1017

Fig. 14

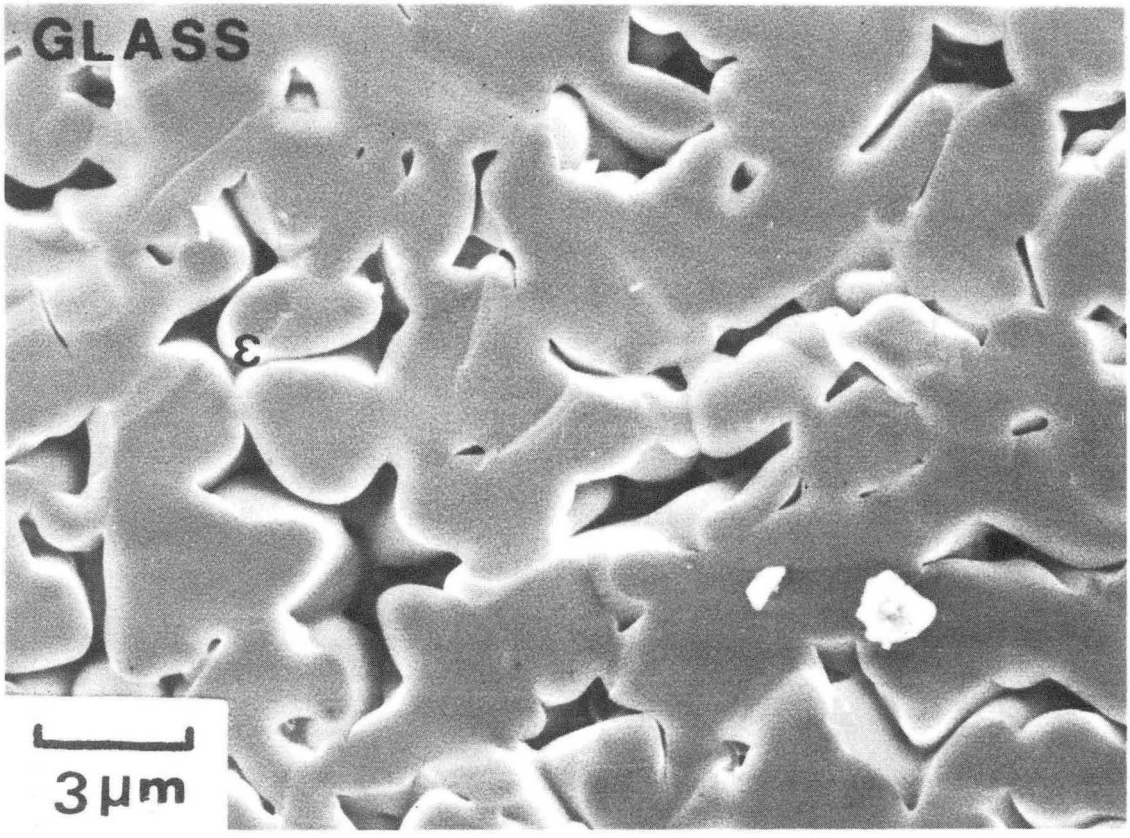

XBB 857-5478A

Fig. 15

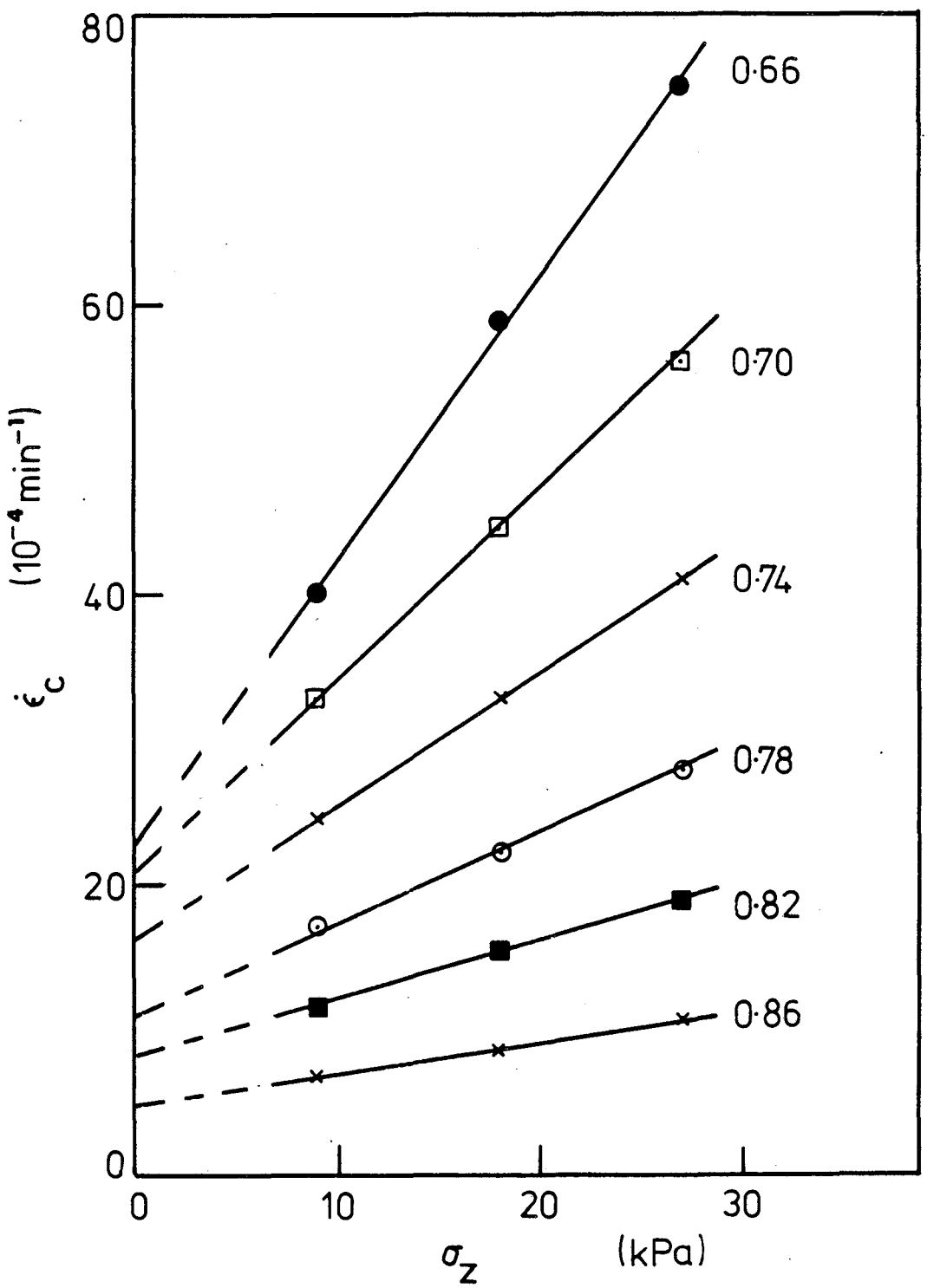

XBL 8510-4447

Fig. 16

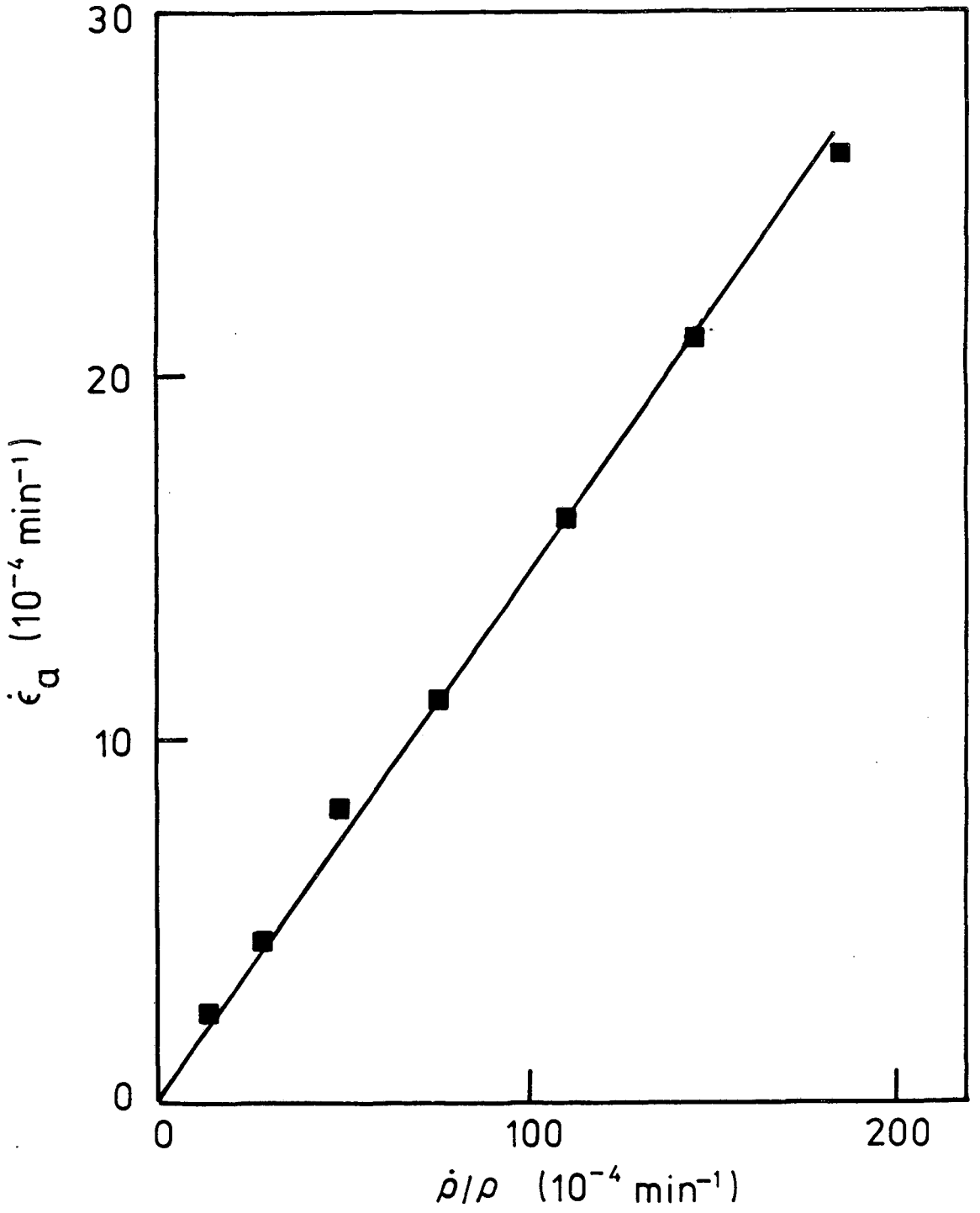

XBL 873-1018

Fig. 17

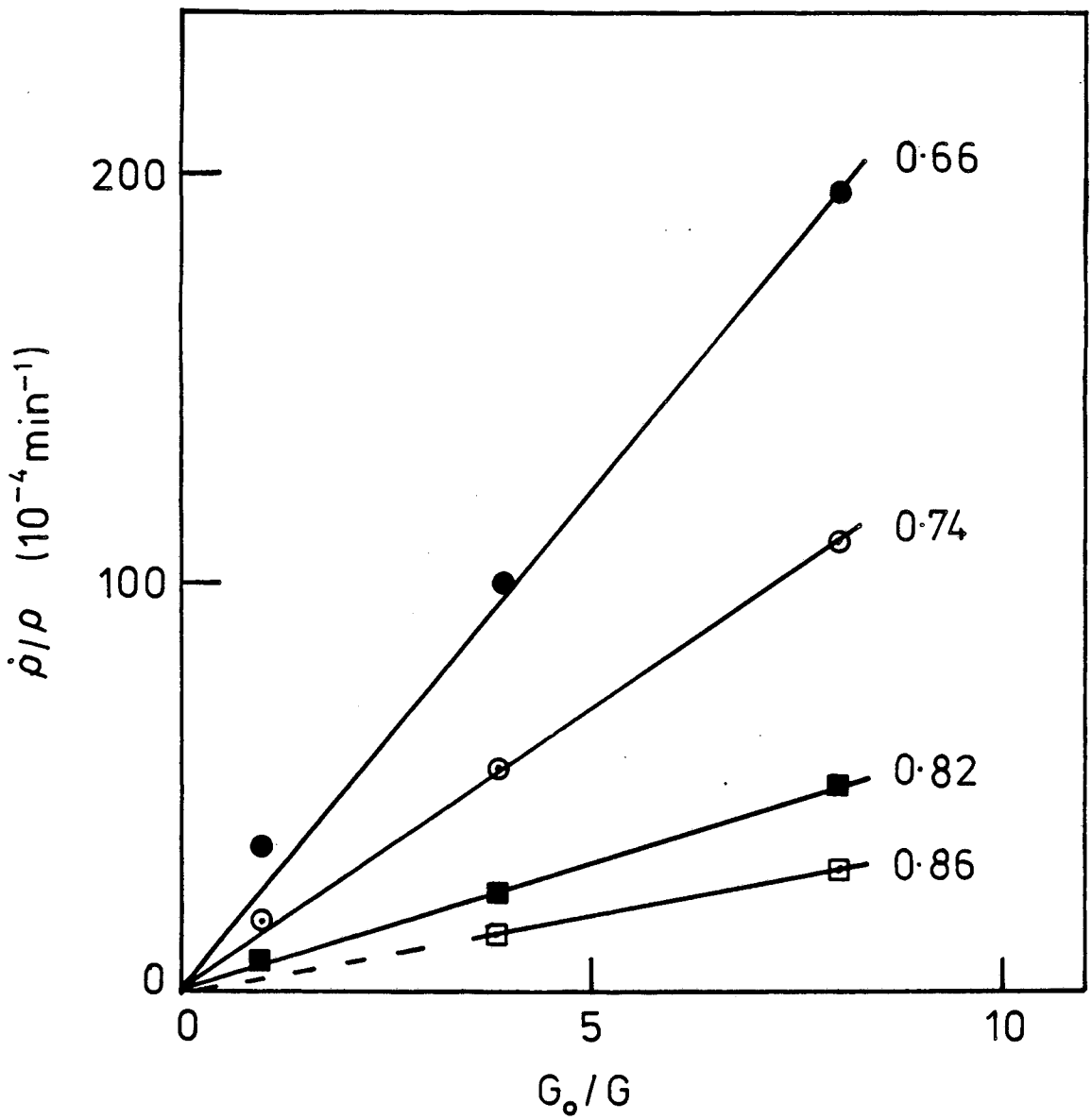

XBL 873-1019

Fig. 18

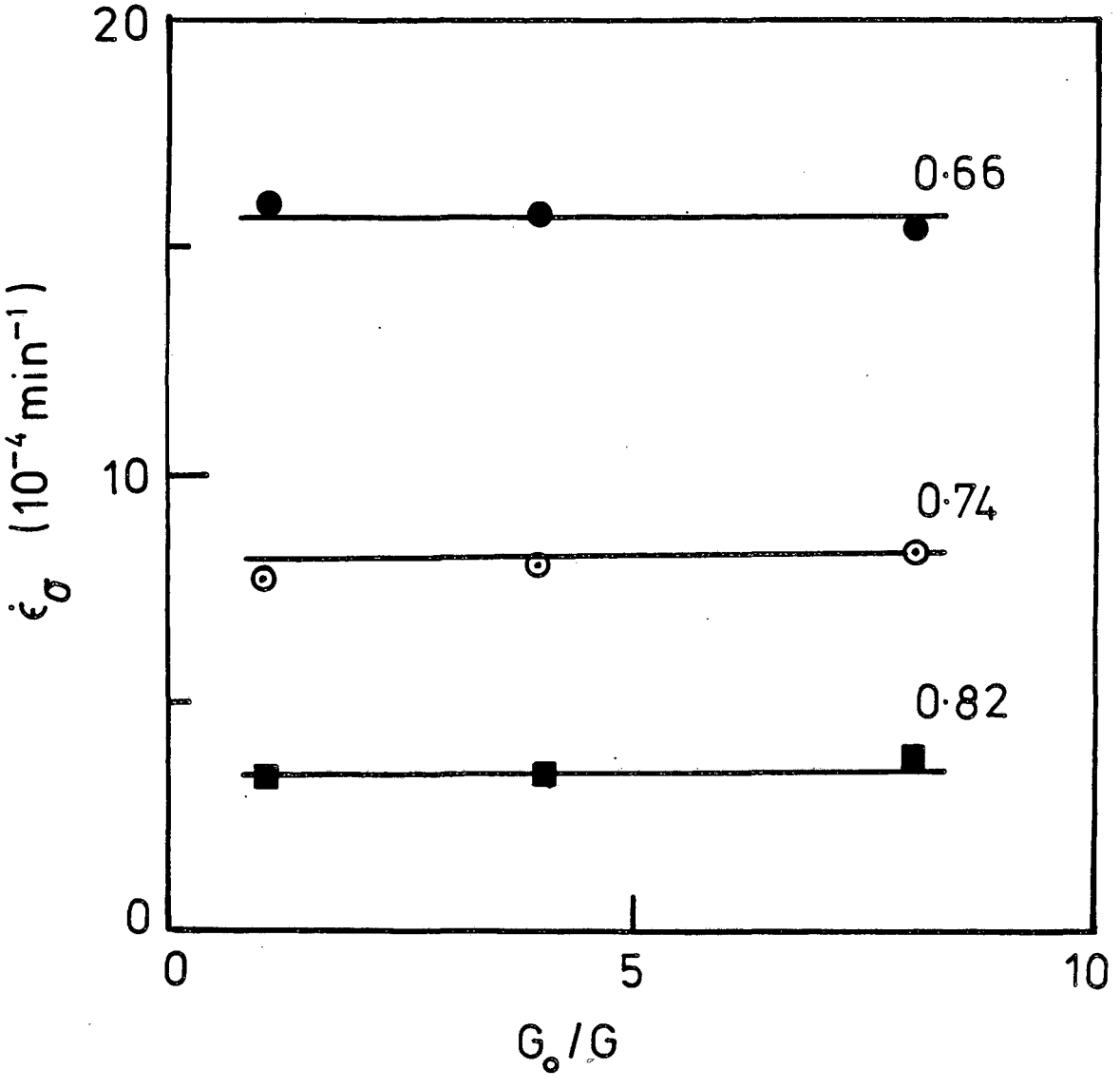

XBL 873-1020

Fig. 19

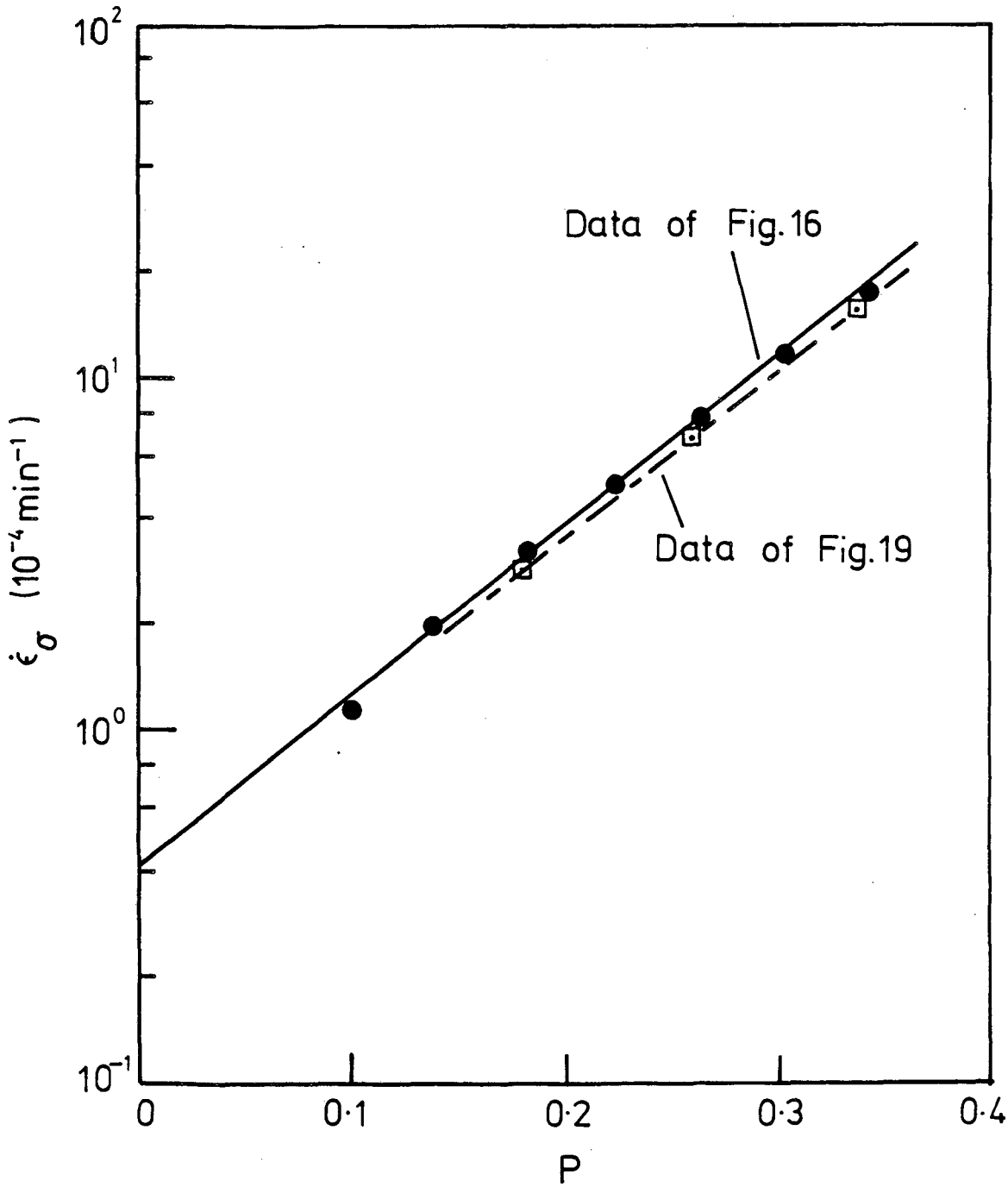

XBL 873-1021

Fig. 20

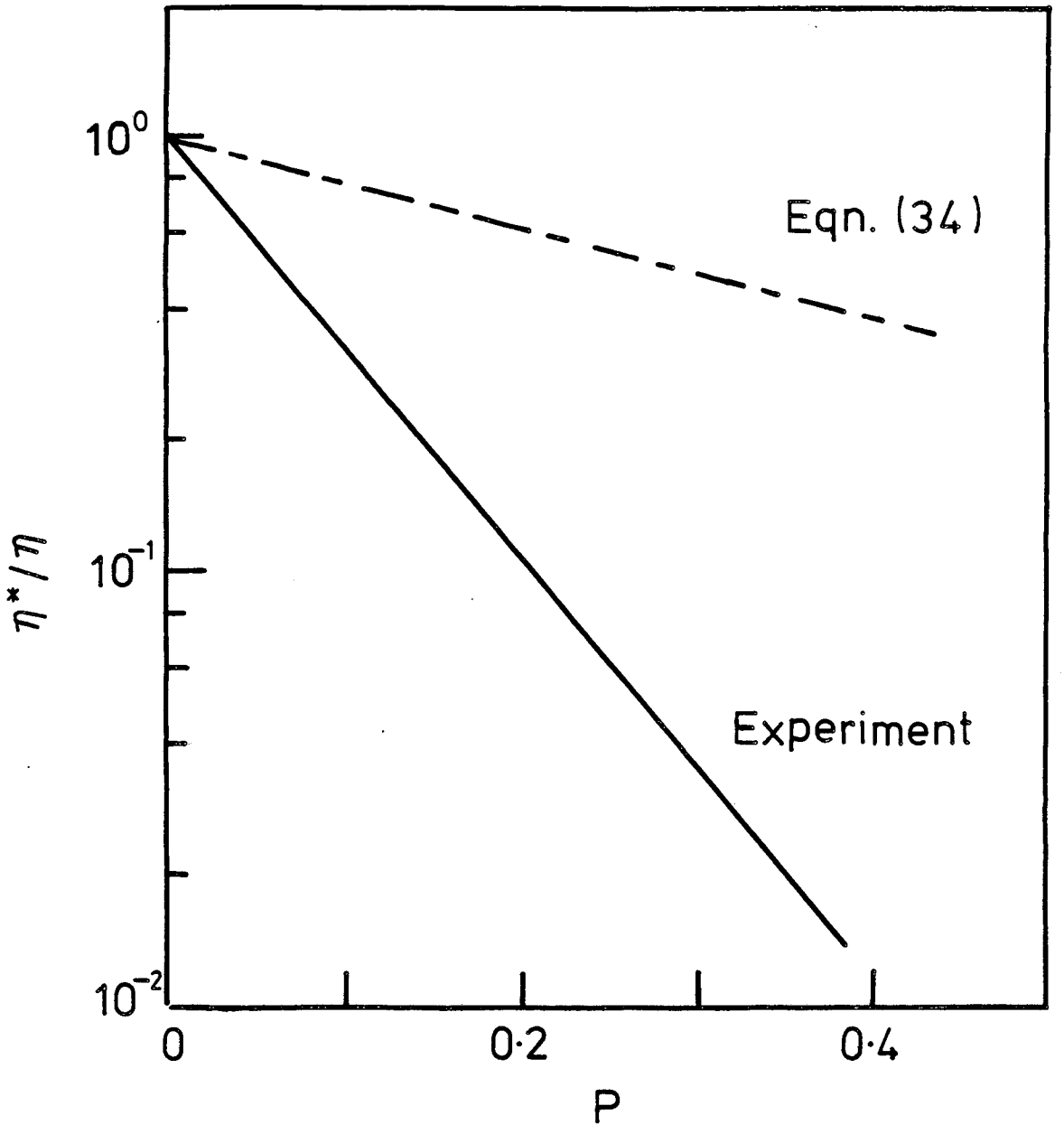

XBL 873-1022

Fig. 21

This report was done with support from the Department of Energy. Any conclusions or opinions expressed in this report represent solely those of the author(s) and not necessarily those of The Regents of the University of California, the Lawrence Berkeley Laboratory or the Department of Energy.

Reference to a company or product name does not imply approval or recommendation of the product by the University of California or the U.S. Department of Energy to the exclusion of others that may be suitable.

LAWRENCE BERKELEY LABORATORY
TECHNICAL INFORMATION DEPARTMENT
UNIVERSITY OF CALIFORNIA
BERKELEY, CALIFORNIA 94720